Publ. Astron. Soc. Japan (2016) 68 (SP1), S1 (1–24)
doi: 10.1093/pasj/psw016
Advance Access Publication Date: 2016 April 21

The MAXI/GSC Nova-Alert System and results of its first 68 months

Hitoshi Negoro,[1,*] Mitsuhiro Kohama,[2,†] Motoko Serino,[3] Hiroki Saito,[1] Tomonori Takahashi,[1] Sho Miyoshi,[1] Hiroshi Ozawa,[1] Fumitoshi Suwa,[1] Masato Asada,[1] Kosuke Fukushima,[1] Satoshi Eguchi,[4,‡] Nobuyuki Kawai,[5] Jamie Kennea,[6] Tatehiro Mihara,[3] Mikio Morii,[3,§] Satoshi Nakahira,[7] Yuji Ogawa,[8] Aya Sugawara,[1] Hiroshi Tomida,[9] Shiro Ueno,[9] Masaki Ishikawa,[10] Naoki Isobe,[9] Taiki Kawamuro,[4] Masashi Kimura,[2] Takahiro Masumitsu,[1] Yujin E. Nakagawa,[9] Motoki Nakajima,[11] Takanori Sakamoto,[12] Megumi Shidatsu,[3] Mutsumi Sugizaki,[3] Juri Sugimoto,[3] Kazuhiko Suzuki,[1] Toshihiro Takagi,[3] Kazuki Tanaka,[1] Yohko Tsuboi,[13] Hiroshi Tsunemi,[14] Yoshihiro Ueda,[4] Kazutaka Yamaoka,[15,16] Makoto Yamauchi,[8] Atsumasa Yoshida,[12] and Masaru Matsuoka[3]

[1]Department of Physics, Nihon University, 1-8 Kanda-Surugadai, Chiyoda-ku, Tokyo 101-8308, Japan
[2]Institute of Space and Astronautical Science (ISAS), Japan Aerospace Exploration Agency (JAXA), 2-1-1 Sengen, Tsukuba, Ibaraki 305-8505, Japan
[3]MAXI team, Institute of Physical and Chemical Research (RIKEN), 2-1 Hirosawa, Wako, Saitama 351-0198, Japan
[4]Department of Astronomy, Kyoto University, Kitashirakawa-Oiwake-cho, Sakyo-ku, Kyoto 606-8502, Japan
[5]Department of Physics, Tokyo Institute of Technology, 2-12-1 Ookayama, Meguro-ku, Tokyo 152-8551, Japan
[6]Department of Astronomy and Astrophysics, The Pennsylvania State University, University Park, PA 16802, USA
[7]Human Spaceflight Technology Directorate, Japan Aerospace Exploration Agency (JAXA), 2-1-1 Sengen, Tsukuba, Ibaraki 305-8505, Japan
[8]Department of Applied Physics, University of Miyazaki, Gakuen-Kibanadai-Nishi, Miyazaki, Miyazaki 889-2192, Japan
[9]Institute of Space and Astronautical Science (ISAS), Japan Aerospace Exploration Agency (JAXA), 3-1-1 Yoshinodai, Chuo-ku, Sagamihara, Kanagawa 252-5210, Japan
[10]School of Physical Science, Space and Astronautical Science, The Graduate University for Advanced Studies, 3-1-1 Yoshinodai, Chuo-ku, Sagamihara, Kanagawa 252-5210, Japan
[11]School of Dentistry at Matsudo, Nihon University, 2-870-1 Sakae-cho-nishi, Matsudo, Chiba 271-8587, Japan
[12]Department of Physics and Mathematics, Aoyama Gakuin University, 5-10-1 Fuchinobe, Chuo-ku, Sagamihara, Kanagawa 229-8558, Japan
[13]Department of Physics, Chuo University, 1-13-27 Kasuga, Bunkyo-ku, Tokyo, 112-8551, Japan

[14]Department of Earth and Space Science, Osaka University, 1-1 Machikaneyama, Toyonaka, Osaka 560-0043, Japan
[15]Department of Particle Physics and Astronomy, Nagoya University, Furo-cho, Chikusa-ku, Nagoya, Aichi 464-8601, Japan
[16]Solar-Terrestrial Environment Laboratory, Nagoya University, Furo-cho, Chikusa-ku, Nagoya, Aichi 464-8601, Japan

*E-mail: negoro.hitoshi@nihon-u.ac.jp
†Present address: Mitsubishi Space Software Co., Ltd., MSS Fujizuka Bldg. 792, Kamimachiya, Kamakura, Kanagawa 247-0065, Japan.
‡Present address: Department of Applied Physics, Faculty of Science, Fukuoka University, 8-19-1 Nanakuma, Jonan, Fukuoka 814-0180, Japan.
§Present address: Research Center for Statistical Machine Learning, The Institute of Statistical Mathematics, 10-3 Midori-cho, Tachikawa, Tokyo 190-8562, Japan.

Received 2015 December 30; Accepted 2016 February 2

Abstract

Various transient phenomena on a timescale ranging from seconds to days appear at unexpected sky positions in X-rays. MAXI, Monitor of All-sky X-ray Image, on the International Space Station has been monitoring about 95% of the sky a day and has detected transient objects since 2009 August. Here, we describe quasi-real-time data processing systems of MAXI and a subsequent nova-alert system to find transient objects, and present the capabilities for the nova-alert system to detect transient events with excess fluxes from $\gtrsim$80 mCrab in a single scan transit to $\gtrsim$8 mCrab for 4 d, and to send prompt alert information to the world in less than 30 s after the onboard detection of a burst, making the best use of the International Space Station (ISS) real-time network. We also report on highlights of scientific results obtained with the system until the end of the first extended mission phase, 2015 March. Including 15 X-ray novae solely or independently discovered, we have reported on 177 transient phenomena, such as X-ray bursts, outbursts, and state transitions of X-ray binaries and X-ray flares from active stars and blazars, via the Astronomer's Telegram, and on 63 burst phenomena of other types via the Gamma-ray Coordinates Network. We summarize the results of these transient sources and phenomena focusing on the detections with the nova-alert system, and some new transients yet unpublished or requiring attention.

Key words: galaxies: active — gamma-ray burst: general — stars: variables: general — X-rays: binaries — X-rays: general

1 Introduction

MAXI, Monitor of All-sky X-ray Image (Matsuoka et al. 2009a, hereafter M09), is the first payload attached to the Exposed Facility (EF) of the Japanese Experiment Module (JEM), Kibo, on the International Space Station (ISS). MAXI is also the first astronomical mission on the ISS, and a unique modern X-ray observatory only for the all-sky X-ray survey.

After the X-ray All Sky Monitor on the Ginga satellite (Ginga/ASM, Tsunemi et al. 1989) and the All-Sky Monitor on the Rossi X-ray Timing Explorer (RXTE/ASM, Levine et al. 1996), which worked until 2012 January 5, MAXI has been the only all-sky X-ray monitor in the soft X-ray band. INTEGRAL/JEM-X (Lund et al. 2003; Westergaard et al. 2003) also has a wide field of view, but it hardly observes all the sky. Very recently, ASTROSAT (Singh et al. 2014) was launched on September 28, and its all-sky monitor, the Scanning Sky Monitor (SSM), has just started its operation. On the other hand, the currently operating INTEGRAL/IBIS (Mereghetti et al. 2003), Swift/Burst Alert Telescope, BAT (Gehrels et al. 2004; Krimm et al. 2013b), and Fermi/Gamma-ray Burst Monitor, GBM (Meegan et al. 2009; Case et al. 2011) are

all for the detection of transient events in the hard X-ray band, mainly to detect gamma-ray bursts (GRBs). Therefore, MAXI has played an important role in finding transient objects and monitoring the sky in the soft X-ray band.

In the soft X-ray sky, there are various transient events on various timescales, e.g., X-ray bursts, prompt and afterglow emission of GRBs, X-ray flares from young stellar objects and main sequence stars, fast X-ray flares from neutron-star and massive-star binaries (e.g., Supergiant Fast X-ray Transients, SFXT), X-ray outbursts and state transitions of black hole candidates and neutron stars, and active galactic nuclei (AGNs) flares. MAXI, with the highest sensitivity of all-sky-monitors to date and the quasi-continuous real-time ISS network, can provide fast alert information useful for multi-wavelength follow-up observations for these events.

The real-time monitoring by scanning the sky from the ISS requires data processing systems that are different from those of previous X-ray satellites. We designed the ground software system in around 2000, taking account of the fast development of computer technologies (Negoro et al. 2004). The MAXI data processing system consists of the following four components: (i) data processors (DPs) in orbit; (ii) the data storage and processing system (MAXI database, hereafter MAXI-DB); (iii) the (X-ray) nova-alert system consisting of a real-time transient monitor (nova-search) and an alert system at JAXA's Tsukuba Space Center (TKSC/JAXA); (iv) the public data archival system at RIKEN.[1] Here, we describe these data processing systems to find various transient events, and summarize their five-year scientific results.

MAXI has two kinds of X-ray cameras: the Gas Slit Cameras (GSC) with a field of view of $1^\circ.5 \times 160^\circ$ (Mihara et al. 2011a; Sugizaki et al. 2011), and the Solid-state Slit Cameras (SSC) with a field of view of $1^\circ.5 \times 90^\circ$ (Tsunemi et al. 2010; Tomida et al. 2011). SSC has two-dimensional CCD cameras, but only one positional information of the CCD chips is used in the ordinary operation. GSC and SSC data hence can be treated in the same manner in the context of this paper. However, here we mainly describe the systems for GSC, because SSC data suffer from various background effects and it has been difficult to use the data for the transient search. The SSC alert system has also been under development, as described in Fukushima et al. (2014).

MAXI was successfully launched with the space shuttle Endeavour on 2009 July 15 (UT), and loaded onto the JEM of the ISS. After the X-ray cameras were turned on during 2009 August 11–18, MAXI has continuously monitored about 85% of the sky every ~92 min, and more than 95% in a day (Sugizaki et al. 2011). Each region of the sky is observed once or occasionally twice in one ISS orbital cycle, and typically 16 times in a day. The scanning duration for a point source is 40–150 s depending on the source acquisition angle (see figure 8 in Sugizaki et al. 2011).

In the following section, we describe data transmission from the ISS to the ground, which limits the prompt alert notification using the ISS network. The functionalities of the MAXI-DB and the position determination method for each photon are described in section 3. In section 4, the real-time transient monitor and alert system are explained in some detail. More detailed information on the development can be found in previous papers (Negoro et al. 2004, 2008, 2010a). Finally, the summary of transient events detected and some examples, already reported onto The Gamma-ray Coordinates Network (GCN) and/or The Astronomer's Telegram (ATel), are shown in section 5

2 Data transmission from the ISS

2.1 Network and network interfaces

The on-board DP compiles MAXI data, and transmits to the NASA ground stations through the relay satellite, Tracking and Data Relay Satellite (TDRS), which is referred to as the NASA link (figure 1). The ICS (Inter-orbit Communication System) link through the Data Relay Test Satellite (DRTS) was also available (see also Ishikawa et al. 2009 for more detail), but most data have been downloaded through the NASA link.

MAXI uses two network interfaces on the ISS: low-speed Mil-1553b and medium-speed (med-speed) Ethernet. Data with full information, for instance, 64-bit GSC event data and house-keeping data (Mihara et al. 2011a), are transmitted via the med-speed interface. The identical, but limited by an energy range (e.g., 2–20 keV), 64-bit data are transmitted also via the low-speed interface as a redundant system. However, since the low-speed interface has a limited transfer rate of usually 50 kbps, which is 1/5 of that of the med-speed interface, degraded 32- or 16-bit GSC event data with the time resolution of 1 s instead are transmitted in some cases via the low-speed interface.[2]

When both the relay satellites are available, data using the low-speed interface (hereafter, 1553b data) are transmitted in parallel through both the NASA and ICS links, whereas data through the med-speed interface (Ethernet data) are transferred through the alternative link. On the other hand, when none of the relay satellites is available, data through both the interfaces are stored on the on-board data recorders, i.e., the High Rate Communication Outage Recorder (HCOR) for the NASA link and/or the High Rate Data Recorder (HRDR) for the ICS link. Basically, the

[1] ⟨http://maxi.riken.jp⟩.

[2] In reality, the 16-bit GSC event data mode has not been used yet.

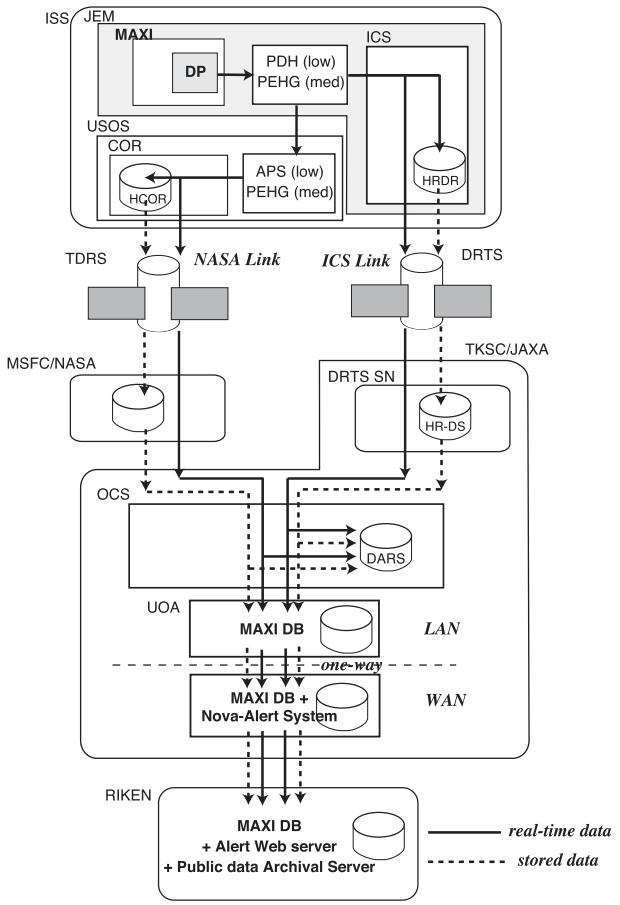

Fig. 1. Schematic view of the data-flow from MAXI to the ground software systems. Abbreviations not given in the main text are APS (Automated Payload Switch) and USOS (Uni States Orbital Segment).

low-speed interface is available most of the time and robust. Our nova-alert system uses the 1553b data via the low-speed interface in order to maximize the chance of detecting potential transient events, even though it means that the data quality of each event is sometimes degraded.

All the data are downloaded and stored in a database in the Operations Control System (OCS) at TKSC/JAXA, and transferred to our MAXI databases for 1553b and Ethernet data (separate databases for security reasons) in the User Operating Area (UOA), passing through a one-way data transfer system.

2.2 Time delay

It takes about 3–5 s to transmit real-time 1553b data from the X-ray detection to the MAXI-DB system on the ground: the DP compiles the data to the MIL-STD-1553b message formats every second, and sends them to the JEM payload bus. The Payload Data Handling Unit (PDH) collects the payload data every second. It takes further a few seconds to reach the OCS from the PDH. Ethernet data are promptly sent to the Payload Ethernet Hub/Gateway (PEHG), with

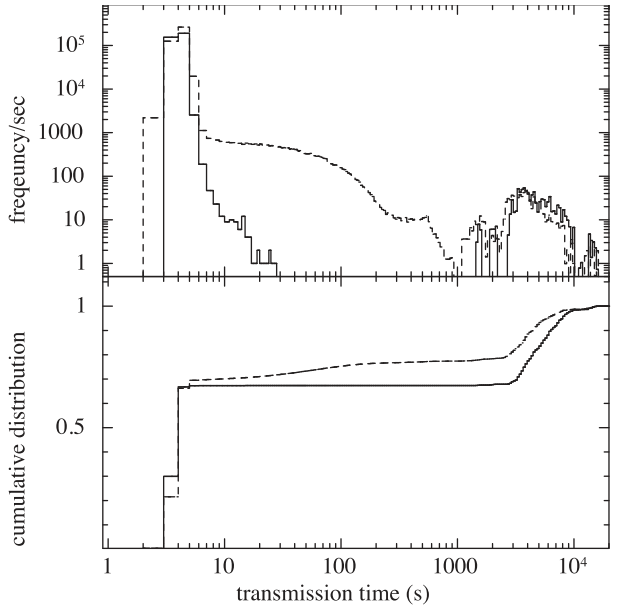

Fig. 2. Frequency distributions of the transmission time of 1 s telemetry (experiment) data from MAXI to the MAXI-DB at TKSC using the 1553b interface (upper panel) and their cumulative distributions (lower panel). Data were obtained on 2009/09/15–20 (solid line), and on 2010/09/15–21 (dashed line). The transmission time is estimated from the time difference between the DPTC time (1 s unit, subsection 3.2) of the telemetry data and time stamp of the files saved in the MAXI-DB, resulting in 1 s ambiguity.

a transmission time that is faster than the 1553b data by a few seconds. It then takes less than 1 s for the MAXI-DB system to obtain the data from the OCS.

Figure 2 shows the observed frequency distributions of the arrival time delay of 1553b telemetry data. About 70% of data are transferred as real-time data during the *real-time* contact with the ground. The data obtained outside of the contact are temporarily stored in the HCOR on the ISS (referred to as the COR data), and are eventually sent to the ground in the next contact, resulting in a secondary peak at around 3000–5000 s in the distributions. Delays from 10 s to 1000 s, which were hardly seen at the beginning of the operation in 2009 (solid line), were due to traffic jams in recording the real and COR data that were rushing into the MAXI-DB simultaneously.[3]

3 MAXI database system

3.1 Functionality and structure

In this section, we briefly describe the MAXI-DB (data storage and processing) system and its functionality. The MAXI-DB is not simply a database for storing the data, but also has the functionality to retrieve, process, and deliver the data (Negoro et al. 2004, hereafter N04). The main

[3] The situation deteriorated until the problem was fixed in 2015 November.

parts of the system are designed at RIKEN, and coded in Java by SEC.[4] Some parts which process the data are in the C language in order to use, for instance, NASA's HEAsoft libraries.[5] The database management system (DBMS) used is PostgreSQL.[6]

The MAXI-DB involves a "photon-event" database using the DBMS (N04). Simple camera design consisting of the collimator and one-dimensional detectors of MAXI (M09) enables us to determine the direction of each incoming X-ray photon. Being different from other astronomical databases, the MAXI-DB stores all the data in the database, and does not include any tags or links to external files out of the database. This is mainly because X-ray photon data of an object are saved in many separate telemetry files because of the scanning observations. In the MAXI-DB, each X-ray photon event is stored as one data record in the database. With the help of the index functionality of the DBMS, any data required to issue prompt alerts can usually be retrieved from all the stored data sets in less than 1 s.

3.2 Real-time processing and position determination

The MAXI-DB receives 1 s telemetry data from the OCS every second, and decomposes the data into individual data components, which include not only *raw* X-ray event data, but also attitude information calculated from the on-board Visual Star Camera (VSC) and three-axis Ring Laser Gyro (RLG) (Ueno et al. 2009), and time information from the on-board GPS. All the decomposed data are stored into the PostgreSQL database in less than one second.

For each X-ray event, the detection time, energy, and incoming direction are promptly calculated in the MAXI-DB by using the decomposed data and calibration data. The calibration data are based on ground calibration experiments and flight data (Sugizaki et al. 2011).

For GSC data, the positional accuracy determined in that way is basically the same as that of the public data products at RIKEN, currently $0.^{\circ}1$ (90% containment radius). The precise time of the data, however, cannot be obtained in real time because the GPS signal necessary for the correction sometimes cannot be obtained in orbit and because jitters of the GPS clock and the on-board free-run clock counter (Mihara et al. 2011a) result in an ambiguity of 1 s. Thus, the trigger time in UTC described in e-mail notifications (subsection 4.4) is calculated by assuming that the DPTC time is equal to the GPS time, even though the DPTC time and GPS time have a discrepancy (of at most 24 s on 2012 July 12).[7] However, those reported onto the GCN or the ATel usually achieve an accuracy of less than 1 s after extrapolation from the past timing data is applied.

Each photon direction typically has errors of $1.^{\circ}5$ in the scan direction and $\sim 2^{\circ}$ in its orthogonal direction at full width at half-maximum (FWHM), corresponding to the point spread function (PSF) of the camera. We define the direction of each photon as the center of the field of view (FOV) at the detected position on the detector. As a result of this definition, the photons from a single source detected in a 1 s long observation window yield a shape of a straight line orthogonal to the scan direction in the resultant image.

We note that for a very short burst event compared to the scan duration the error in the scan direction can be very large because the incident angle of detected photons to the scan direction is limited only by the slat collimator and the detector has no positional sensitivity to the scan direction orthogonal to the direction of carbon wires in the detector. In the worst case, such as those with a duration of less than a few seconds, the error is up to 3° independently of the intensity [some examples are presented in Morii et al. (2010a) and Serino et al. (2014a)].

The resultant *processed* X-ray event data are sent to the following nova-search systems, about 4 s after the MAXI-DB receives the telemetry data. The processed data are also simultaneously stored in the database.

4 The nova-alert system

By using the processed data described in subsection 3.2, a transient event search is sequentially performed on the (X-ray) nova-alert system on the ground. The nova-alert system consists of a real-time transient monitor (hereafter, nova-search) and an alert system (Negoro et al. 2010a). The nova-search system finds possible transient events judging from count increases in sky-map pixels, and sends the information to the alert system. The alert system checks the confidence of the events, and sends an e-mail alert notification to MAXI duty scientists and subscribers to the MAXI mailing list (ML).[8] These systems have been developed at Nihon University with the support of JAXA and RIKEN.

4.1 Nova-search system as a real-time X-ray monitor

A nova-search program receives event data from the MAXI-DB every second when the data are being downloaded, and

[4] Systems Engineering Consultants Co., Ltd.

[5] ⟨http://heasarc.gsfc.nasa.gov/lheasoft⟩.

[6] ⟨http://www.postgresql.org⟩.

[7] Data Processor Time Counter: DP clock counter incremented every second, initialized by the GPS clock. DPTC can be converted to UTC with an accuracy of 50 μs on the ground a few days after the observation.

[8] We have the following five MLs: `AGN`, `Nova-cv`, `Supernova`, `X-ray-star`, and `New-transient`. See ⟨http://maxi.riken.jp/mailman/listinfo⟩.

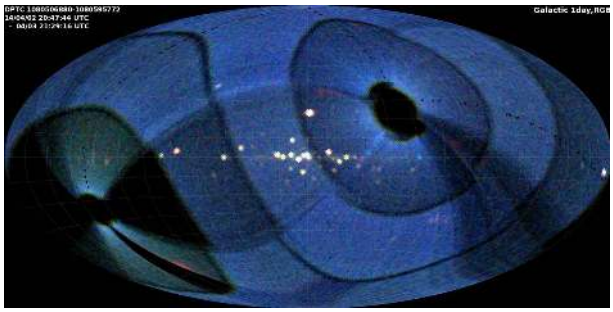

Fig. 3. Example of a false-color (1 d) X-ray all-sky image produced by the nova-search system. Such an image is produced every orbit, 4 orbits, 1 d, and 4 d using data of the latest time bins of the corresponding timescale bins. Source activities including spectral changes are monitored through the web interface, MAXI All-Sky Image Viewer (MASIV).

accumulates the data into curved-surface *pixels* on the celestial spherical coordinates, partitioned with the HEALPix library (Górski et al. 2005). Each pixel covers the same surface area as every other pixel. The program performs timing analysis to detect a transient event and draws the sky-map using the accumulated data. Also, processes for receiving and saving data are run in parallel using the PTHREAD library (Saito 2008) and the GThread library in GTK+ (Ozawa 2011).[9]

The number of spherical surface pixels is $12 \times 64^2 = 49152$ (the HEALPix NSIDE parameter is 64), and the corresponding spatial resolution is about $0.^{\circ}91$, about half of the FWHMs of the PSF of GSC. MAXI scans the sky at a rate of $0.^{\circ}017$–$0.^{\circ}065$ s^{-1} and the scan duration for a point source is 40–150 s (depending on the acquisition angle β, see Sugizaki et al. 2011). A larger number of pixels yield better spatial resolution of the sky image, but a smaller number of photons are accumulated in one pixel, resulting in less sensitivity for the detection of time-variable events.

The system displays a real-time color intensity map in one of four energy bands described below, or a false-color image representing X-ray count rates in the low (2–4 keV, red), medium (4–10 keV, green) and high (10–20 keV, blue) energy bands using GTK+ (Ozawa et al. 2010; Negoro et al. 2010a; see also figure 3).

The nova-search systems have been working as real-time X-ray monitors at TKSC/JAXA since the beginning of the operation, leading to the first report of GRB 090831 to the GCN 13 days after the normal operation was started (Matsuoka et al. 2009b).

4.2 Timing analysis to find transient events

The system investigates time-series data in each sky-map pixel in various timescale bins to detect various types of transient events. Each pixel has 32 light curves (eight timescales × four energy bands), each of which consists of 10 time bins where time gaps are allowed between bins, plus sliding-window bins for some timescale bins. The timescales, namely the size of the bins, of the curves are as follows: four short timescale bins (1, 3, 10, and 30 s bins during one scan transit) and four long ones [1-scan (40–150 s), 4-orbits, 1 d and 4 d bins, where a 1-orbit (= 1 or 2 scan transits in ∼92 min) bin was used instead of 4 d bin until 2010 December]. The four energy bands are the low, medium, and high energy bands described before and the 3–10 keV band as the highest S/N (signal-to-noise ratio) band for ordinary energy spectral sources.

For the curves of the 3 s bin and the bins longer than the 1-scan bin, sliding-window time bins for evaluating the time variability have been introduced, to prevent a sudden change of the detection criteria that accompanies the change of the time bin (Ozawa et al. 2010). The sliding-window bins are constructed from the shorter time bins.

Every second, the system approximately integrates exposure time in each spherical surface pixel in the FOVs of active detectors and the geometrically corrected effective area of the detectors (Miyoshi 2010). Furthermore, since 2011 May 24, the background counts have been subtracted in real time.

The background counts are estimated from recent (30–40 s) count rates at the same detector position with a width of ∼3° and from the data of the entire (∼80° in width) detector for the latest 1 s to detect a sudden increase of the background (often due to a drop of the high-voltage of the camera before entering high background geometrical regions). The recent count rates are evaluated in the following two ways: simply averaged count rates of recent 30 s data, or expected count rates obtained by the linear fit to count rates of recent 40 s data. In both methods, bright source regions are excluded before the calculations are made.

Many fake events used to be detected, not only due to solar activities and charged particles, but also due to large background variations in some sky-pixel regions by a factor of more than two in a scan-by-scan observed at different geomagnetic positions (e.g., Sugizaki et al. 2011) and to gradual increase of background rate in some sky-pixel regions observed at different detector positions resulting from the precession of the ISS orbit on timescales longer than 1 d. The real-time subtraction of the background greatly reduces such fake events and enables us to set lower criteria, almost comparable to the detection limits (table 1).

If at least one X-ray event is detected in an energy band in a sky-map pixel, the system calculates the expected average numbers of counts of the pixel in all the timescale bins of

[9] ⟨http://www.gtk.org⟩.

Table 1. Example of trigger criteria P set in the nova-search system.

Time bins	3–10 keV	2–4 keV†	4–10 keV	10–20 keV
1 s	10^{-3}	10^{-4}	10^{-3}	10^{-3}
3 s	10^{-3}	$10^{-3.5}$	10^{-3}	10^{-3}
10 s	10^{-3}	$10^{-3.5}$	10^{-3}	10^{-4}
30 s	10^{-3}	$10^{-3.5}$	10^{-3}	10^{-4}
1 scan	10^{-3}	10^{-4}	10^{-3}	10^{-4}
	(80)*	(80–120)	(100)	(400)
4 orbits	10^{-3}	10^{-4}	10^{-3}	10^{-4}
	(25)	(50–70)	(35)	(200)
1 d	10^{-4}	10^{-4}	10^{-3}	10^{-4}
	(12)	(25)	(15)	(100)
4 d	10^{-4}	10^{-8}	10^{-3}	10^{-5}
	(7)	(15)	(8)	(50)

*Values in parentheses are corresponding (approximate) 3σ detection limits in mCrab units estimated in the nova-search system.

†Criteria in the 2–4 keV band are sometimes set at much smaller values to avoid solar X-ray flares.

the corresponding energy band(s), and evaluates the criteria to detect a significant variation. By taking accumulated exposure time of the pixel at that time into account, the expected average numbers of counts are estimated from average count rates in the past nine time-series bins of the same timescale bin for the long-timescale bins, or in the past nine 1-scan time-series bins for the short-timescale bins.

The criteria are promptly calculated by the fast calculation algorithm based on Poisson statistics (see appendix 1 for more detail). The criteria are given by chance probabilities, typically ($P =$) less than or equal to 10^{-5} to 10^{-3} (see table 1 for more detail) for the background (and source count) fluctuation to cause the observed number of counts. We further impose a criterion that the number of counts should be more than 4 counts s^{-1} or 5 counts bin^{-1} for each time and each energy bin. If the number of counts of the pixel equals or exceeds the criterion (*trigger* condition), the system sends the information to the alert system. We note that such a transient event search is performed every second in order to find an active source as soon as it emerges.

If the delayed COR data and very occasionally reprocessed data come in, the system deals with the data in the same manner as the real-time data except for a slight difference in the way the background is estimated.[10] In the real-time case, the background was estimated from the preceding nine time-bins (see above). In this case, the system looks at a block of 10 time-bins in each search, and when an event is detected, the background is estimated from the nine time-bins of the block that do not contain the source counts to be evaluated. Namely, all of nine time-bins to be used to estimate the background can be the bins preceding the source event, or all may follow it, or some of them may precede it and the others may follow it. The parallel processing of these and the real-time data has been performed since 2010 December 16 (Ozawa et al. 2010), and the result of this processing implies that some short-term transient events in the COR data before the date might remain unrecognized (e.g., Suwa et al. 2010).

4.3 Alert system

The alert system compiles the information on *triggered* events sent from the nova-search systems, and sends alert information to the world automatically and/or by hand through some MLs delivered from RIKEN.[11] Auto-detection with a single nova-search system and an alert system started on 2009 November 5. Since 2009 December 11, two alert systems for nova-search systems with different criteria and the different background subtraction methods have been running at TKSC. One of the alert systems has also received events from a nova-search system only for a degraded camera, Camera A3, in which the anticoincident counting has not been working. The alert system written in C++ uses HEASoft and ROOT libraries.[12]

If the alert system receives a triggered event at a sky-map pixel from the nova-search systems, the system records the DPTC time of the first received event as the *trigger time*. The system accumulates the numbers of triggered events at the sky-map pixel in each energy band (*accumulated triggered*-event) as far as it receives signals without the interruption for more than 12000 s (>2 orbits). The system also regards adjoining pixel events as one enhanced celestial source event and adds the events to the accumulated triggered-event because a (bright) point source is expected to split into two or more pixels due to the PSF of GSC being broader than the pixel size. For such multipixel events, the system determines the source position from the triggered-count-weighted pixel-center coordinates of HEALPix. For a single-pixel event as mentioned later, the system regards the pixel-center coordinates as the source position.

The system checks every accumulated triggered-event every second. If no further event comes in at the pixel(s) with the accumulated events from the nova-search system(s) for 10 seconds, the system considers the source to be no longer at the center of the FOVs or to have ceased activity (except for a "*Burst*" event, mentioned later). Also, if the accumulated triggered-event satisfies one of the two criteria

[10] Reprocessed data: data which cannot be processed at TKSC automatically due to the loss of the data, and are reprocessed later by using archival data at NASA MSFC.

[11] The socket interface to the GCN has been also implemented, but currently not used.

[12] ⟨https://root.cern.ch⟩.

that (i) the event is split into more than 1 pixel (multipixel condition) and that (ii) the number of triggered events exceeds 15 and the source position lies within 1° from a cataloged (faint) source (single-pixel condition), then the system regards the accumulated triggered-event as a *detected* event and classifies the event as an "*Info*," "*Warning*," "*Alert*," or "*Burst*" event, and sends e-mail alerts to relevant users (Suwa et al. 2010; Suwa 2012).

Info events: MAXI data often suffer from M- and X-class solar flares below 2–3 keV and particle backgrounds while the ISS is approaching the South Atlantic Anomaly. The solar paddles of the ISS sometimes shade X-ray sources or reflect solar X-rays, giving rise to fake events. The system excludes such events as much as possible by using the information on the solar paddle and the ISS position from Earth, which are included in auxiliary data from the ISS and promptly (<1 s) obtained from the MAXI-DB, and on the solar position. The system classifies them as "*Info*" events.

Warning and *Alert* events: all the events considered to be real astronomical transient events are labeled as "*Warning*" or "*Alert*" events. *Alert* events are more significant than *Warning* ones, and have a chance probability of from $P < 10^{-8}$ to $10^{-6.5}$. The relatively low threshold $P(\sim 10^{-3})$ in the nova-search systems gives rise to a number of triggered events (more than one event per second in a high background count rate). The multipixel condition for uncatalogued sources, however, decreases a net chance probability to roughly $(0.1\text{–}1)P^2$, and greatly reduces fake events due to count fluctuations (less than one event per hour on average as expected), especially for *Alert* events.

Burst events: an event is regarded as a "*Burst*" event if the event satisfies the following four criteria: (i) the *Alert*-event criterion is satisfied; (ii) the source position is away from all the catalogued sources by more than 1°; (iii) the number of triggered events is greater than, or equal to, 40; (iv) the event triggers in multiple timescale bins, including short ones, and in multiple energy bands.

The celestial source catalog used in our systems contains sources with a maximum flux of more than 100 mCrab in the past, and is updated by adding nearby flaring stars and newly discovered X-ray sources.[13] The source fluxes in the catalog are updated daily utilizing the MAXI public archival data. The system discards triggered events if the source position is within a certain radius $r_{\rm bs}$ from the position of a known bright source. The radius $r_{\rm bs}$ is determined as $r_{\rm bs}[^\circ] = \log(F_{2-20{\rm keV}}[{\rm mCrab}])$ for $F_{2-20{\rm keV}} \geq 100$ mCrab, otherwise $r_{\rm bs}[^\circ] = 0$, where $F_{2-20{\rm keV}}$ is the flux in the 2–20 keV band. Note that discarding bright sources sometimes results in failure to notice burst events from the sources.

[13] The sources were selected from the Swift/BAT Survey 22-month Catalog (Tueller et al. 2010), the RXTE/ASM Catalog ⟨http://heasarc.nasa.gov/docs/xte/ASM/sources.html⟩, the INTEGRAL General Reference Catalog Ver. 30 ⟨http://www.isdc.unige.ch/integral/science/catalogue⟩, and the ROSAT Bright Source Catalog (Voges et al. 1996).

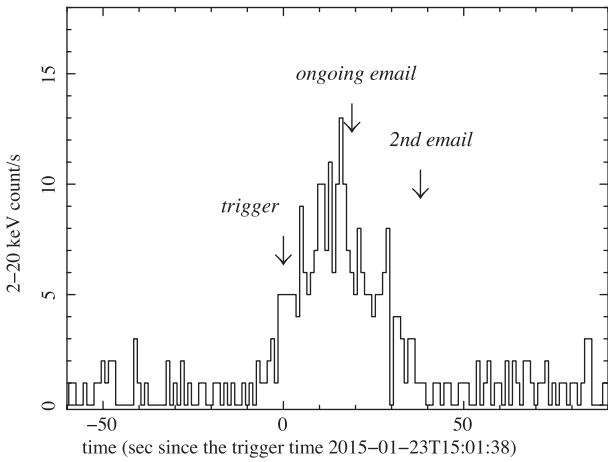

Fig. 4. 2–20 keV light curve of GRB 150123A on which the fastest burst information to the world was issued within 19 s after the trigger shown by the arrow (Fukushima et al. 2015).

4.4 E-mail notification

For a burst event, the alert system automatically sends an alert ("Ongoing Burst") e-mail for a probable GRB to the `New-transient` ML as soon as the event meets all of four criteria of a *Burst* event. The system cannot determine the source position correctly during the scan transit. We hence give a positional uncertainty of 1° in the first e-mail notification. After the scan transit, the system sends an e-mail notification again with a refined position by using all the triggered events.

For a *Warning* or *Alert* event, duty scientists and/or MAXI team members judge whether the event is an astronomical transient event or not, in terms of a flash report and other information described below, and manually send e-mail notifications to the relevant ML if it is worth alerting researchers.

The fastest e-mail notifications to the world were, for instance, 19 s after the trigger time for GRB 150123A (Fukushima et al. 2015; see figure 4), and 21 s for GRB 140818A (Honda et al. 2014). In principle, it is possible to send an e-mail notification within about 10 s for a very bright or short burst. In fact, an (internal) *Alert* e-mail for a short GRB, GRB 150313A (Morooka et al. 2015), was issued only 11 s after the on-board detection (figure 7a). For *Warning* and/or *Alert* events, it usually takes less than 10 min to inform the world of the burst through the MAXI MLs.

Table 2. ATel reports summary: X-ray binaries in our Galaxy, LMC, and SMC.

Type	Outburst		State transition		X-ray burst	Superburst	Brightening, darkening	Mailing list*
	New	Known	New	Known				
BHC	6	6 (13)†	4 (5)	7 (14)	—	—	1	(19)
NS LMXB	4	13 (20)	0	3	3	6	8	(146)
Pulsar	1	18 (42)	0	0	0	0	3	(84)
SFXT	0	2	0	0	0	0	0	(9)
WD	1	0	0	0	—	—	0	(3)
Unknown‡	2(4)	0	0	0	—	—	0	(10)

*The numbers in parentheses are the numbers of e-mail alerts sent to the MAXI ML.
†The numbers and those in parentheses are the numbers of sources and telegrams, respectively, reported on to the ATel.
‡MAXI J1932+091 and MAXI J1619−383 are classified as "new/unknown" here. MAXI J0057−720 and MAXI J1807−228 are "known/pulsar" identified as AX J0058−720 and "known/LMXB" as SAX J1806.5−2215, respectively.

4.5 Post-analyses

The alert system runs a Python script to generate a short web report ("flash report," developed at RIKEN and JAXA) for each detected event. The report includes an image and a light curve in a scan-by-scan, and accumulated images corresponding to the triggered timescales. The reports for the events sent to the ML are stored in the open-access archive on the RIKEN website.[14]

A more precise source position with associated errors and count fluxes, with and without the assumption of constancy in the detected source flux, are obtained by unbinned maximum-likelihood fits to source images with a model, which consists of the detected point source, nearby point sources if they exist, and backgrounds, taking the PSF of the cameras fully into account. (Morii et al. 2010a; also see Appendix of Morii et al. 2016). We usually include these positions in GCN and/or ATel reports. We also investigate the past long-term activity of the source using an on-demand analysis pipeline script (Nakahira et al. 2013b) if necessary.[15] The script also produces an energy spectrum that is useful for investigating the nature of an unknown source.

It takes a few minutes for each of these post-analysis systems to generate the data for a short transient event, and several minutes or more for an event that is detected based on the data with a timescale bin of 1 or 4 d.

5 Results

With the nova-alert system, we have discovered 15 X-ray transients until the end of 2015 March. We have reported on 177 transient events detected with the system to the ATel, and 63 burst events to the GCN circulars. Here, we summarize observational results obtained with the nova-alert system until the end of 2015 March. We summarize the number of ATel and GCN reports by category in tables 2 and 3. (For individual objects, see tables 6–8 in appendix 2.) For detailed scientific results obtained with MAXI data, such as the nature of individual objects, we cite published papers rather than describing the results in detail here. We briefly describe some scientific results which have not yet been published in subsection 5.3.

Table 3. ATel and GCN reports summary: active stars, AGNs, GRBs, and others.

Type	ATel	GCN	Mailing list*
Stars (total)	21 (28)†	1	(70)
dMe/dKe	8 (9)		
RS CVn	8 (10)		
Algol	1 (4)		
YSO	1		
Others	3 (4)	1	
AGNs	6 (10)	—	(14)
GRBs	1	63	
Unknowns	10		

*The numbers in parentheses are the numbers of e-mail alerts sent to the MAXI ML.
†The numbers and those in parentheses are the numbers of sources and reports, respectively.

Before presenting those scientific results, we briefly summarize statistics of the events detected with the nova-alert system in the following subsection.

5.1 Detection limits and positional accuracy

The nova-alert systems have detected time variations of various celestial objects. For instance, in three years from 2012 to 2014, the systems detected seven *Burst* events, 361 *Alert* events, and 3274 *Warning* events. Note that these are real events where fake events are not included. Since about half of the events are detected in both the systems, the systems have detected on average net 0.2 *Alert* events and 2 *Warning* events every day.

[14] ⟨http://www.maxi.riken.jp/alert/novae/index.html⟩.
[15] ⟨http://maxi.riken.jp/mxondem/⟩.

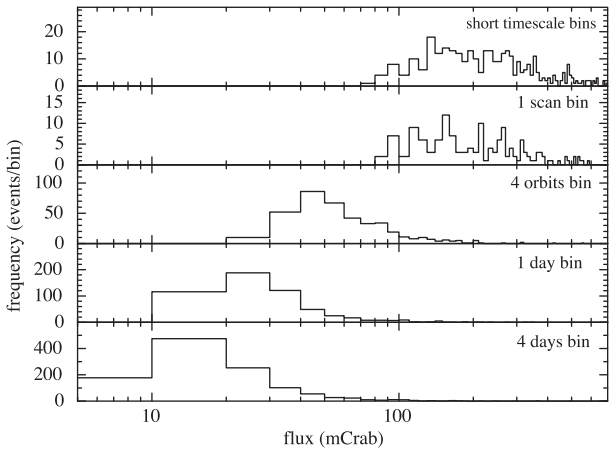

Fig. 5. Frequency distributions of detected excess fluxes in time bins where events were detected with the highest significance. The unit on the vertical axis is events per bin, and 1 bin = 10 mCrab. Only results from *Warning* events detected in 2012–2014, showing the most significant detection in the 3–10 keV or 4–10 keV energy band, are presented. The detected excess fluxes are measured in the nova-search system, and each flux has at most 20%–30% uncertainty. Low significant events with less than 2σ are excluded.

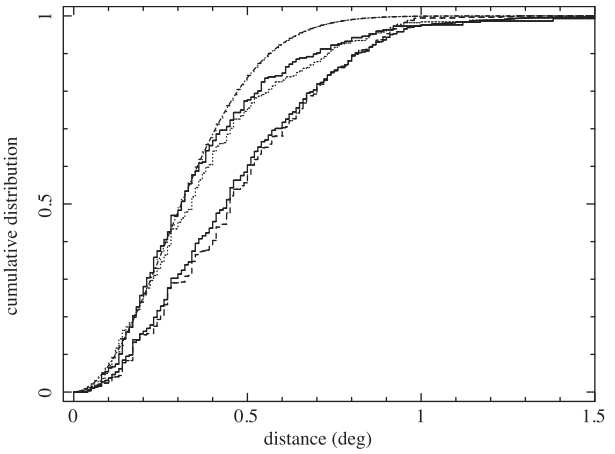

Fig. 6. Cumulative distributions of angular distances between source positions determined in the alert systems and catalogued source positions. Distributions of all the *Warning* events (*lower thick solid line*), *Warning* events detected only in 1 pixel (thin dashed line), *Warning* events in more than 2 pixels (thin dotted line), and *Alert* events (upper thick solid line) are shown. The thin dash-dotted line shows a best-fitting curve via the function C_d (see text). Data are obtained from events detected in 2012–2014.

Figure 5 shows frequency distributions of detected excess fluxes in each timescale bin where events were detected with the highest significance. The lowest-detected fluxes in figure 5 are generally in good agreement with the 3σ detection limits estimated in the nova-search system shown in table 1. Basically, the detection limits are governed by Poisson statistics. Total counts of the Crab in a single scan transit are roughly 200 (150–300) counts in the 3–10 keV band. X-ray photons from a 100 mCrab source spread into one or two pixels near the center of the source position in the nova-search system, and result in 10–15 counts pixel^{-1} corresponding to 3–4σ detection in a single scan transit. We also note that detection limits by the unbiased search, without the single-pixel detection for known sources, are slightly worse, for instance, 15–20 mCrab for 1 d (Suwa 2012).

Figure 6 shows cumulative distributions of angular distances between the (count-weighted) source positions by the alert system and catalogued positions. From the distributions, we obtain the 90% confidence error radii of the positional determination, 0.°81 for *Warning* and 0.°70 for *Alert* events. If we represent the PSF of the camera by a symmetric two-dimensional Gaussian profile $\propto \exp(-r^2/2\sigma^2)$ where r is the angular distance, the cumulative distribution can be represented by $C_d(r) = 1 - \exp(-r^2/2\sigma^2)$ and the 90% confidence error radius is $\sqrt{-2\ln 0.1}\sigma \simeq 2.15\sigma$. Fitting C_d to each of the cumulative distributions gives $\sigma = 0.°37$ for the *Warning* and $\sigma = 0.°30$ for the *Alert* events, and the corresponding 90% confidence error radii are 0.°80 and 0.°65. Note that these are not the final accuracies of the position determination. For final positional accuracies, taking all detected photons and the PSF of the cameras into account, we discuss in subsection 5.3 for new transients.

The estimations of the positional determination accuracy with the function C_d are roughly 2–3 times worse than simple estimations from the central limit theorem, $\sigma_{exp} \simeq \sqrt{(\sigma_P/\sqrt{n})^2 + \sigma_{sys}^2}$ degrees, where σ_P is an approximate standard deviation of the PSF ($\simeq W/2\sqrt{2\ln 2} \sim 0.°7$, where W is the FWHM of the camera, and $1.°5-2°$), n is the total number of counts, and σ_{sys} is the systematic uncertainty ($\sim 0.°05$). For instance, typical *Warning* events with $n \sim 25$ counts of 5σ detection give $\sigma_{exp} \sim 0.°15$, and *Alert* events with $n \sim 100$ counts corresponding to 500 mCrab in a single scan transit give $\sigma_{exp} \sim 0.°09$.

These discrepancies are due to the position determination method based on only triggered pixels with the resolution of $\sim 0.°91$ (e.g., the distribution of single-pixel detections of catalogued sources shown by the dashed line in figure 6), and due to burst or flare detections off the center of the cameras, which is clearly seen as a large discrepancy at $r > 0.°4$ between a C_d curve with $\sigma = 0.°26$ obtained by fitting the distribution of the *Alert* events at $r \leq 0.°4$ (dash-dotted line) and the distributions of highly significant events, *Alert* events (upper solid line) and *Warning* events triggered in more than 2 pixels (dotted line) (also see subsection 3.2).

5.2 Short-term burst and flare events

5.2.1 Gamma-ray bursts

Gamma-ray bursts (GRBs) and X-ray bursts (XRBs) triggered the system in short timescale bins. 63 GRB-like events

(56 prompt emissions and seven afterglows)[16] were detected mostly by the nova-alert system,[17] and we sent 68 circulars to the GCN. 12 Swift/XRT follow-up observations for the positions determined from MAXI observations were carried out usually in less than half a day, and four afterglows (GRB 110213B, 121025A, 130505B, 140818A) and four afterglow candidates (GRB 120510A, 140221A, 150110C, and 150123A) were detected.

The average detection rate for over five years is 10.0 bursts (prompt emission) a year, which is about three times higher than expected before launch, 3.5 bursts per year (Suzuki & the MAXI Team 2009). Seven X-ray afterglows were also detected. The average rate, 1.24 afterglows per year, is smaller than the expectation, 2.4 per year. Serino et al. (2014a) summarized the results of 35 GRBs that MAXI detected until the middle of 2013, and showed that the 20 bursts only MAXI detected tended to have soft energy spectra and low fluxes of less than 10^{-8} erg cm^{-2} s^{-1} (see also Sakamoto et al. 2014).

5.2.2 X-ray bursts and superbursts

A number of X-ray bursts have been detected (e.g., in't Zand 2011). We note again that, as described in subsection 4.3, bright sources with fluxes $\geq$100 mCrab are masked in the nova-alert system. As a result, bursts from those sources are ignored. Through reference to past burst activities obtained by the HETE-2 satellite (Suzuki et al. 2006) and the XRB database MINBAR (Galloway et al. 2008), we usually let researchers know about bursts only through the `X-ray-star` ML. For peculiar bursts or bursts requiring attention as described next, however, we have also reported them to the ATel.

For an X-ray burst (or outburst) from a globular cluster, follow-up observations are necessary for identifying the source, because some globular clusters contain multiple X-ray sources, unresolved with the MAXI cameras. For example, an X-ray burst from M 15 on 2011 May 16 (Morii et al. 2011) was soon identified as new activity of the ultra-compact binary M 15 X-2 by successful Swift/XRT (Heinke et al. 2011), ELVA (Miller-Jones et al. 2011), and Chandra (Sivakoff et al. 2011) follow-up observations.

Currently, eight unusually long X-ray bursts were found in the MAXI data: they lasted more than 1 scan transit ($\geq$23 min or $\geq$92 min) and were identified as superbursts or intermediate-duration bursts (e.g., Strohmayer & Bildsten 2006). The nova-alert system does not have specific functionality for the detection of such long X-ray bursts. We have, however, found five out of the eight superbursts (or intermediate-duration bursts) with the nova-alert system (three automatically, and two manually with nova-search images by eye), and rapidly reported on them to the ATel, except for a superburst from SAX J1747.0−2853 (Chenevez et al. 2011) which was automatically detected but not noticed as a superburst.

A long X-ray burst, triggered on 2011 November 12 and lasting more than half a day was likely the first superburst detection from SAX J1828.5−1037 (Asada et al. 2011). The longest X-ray burst ever observed, probably from SLX 1735−269, was noticed with nova-search images on 2012 December 6 (Negoro et al. 2012b). A superburst from EXO 1745−248 was also manually detected on 2011 October 24 (Mihara et al. 2011b; also see Serino et al. 2012 in detail). On the other hand, it was difficult to notice superbursts from 4U 1820−30 (in't Zand et al. 2011) and Aql X-1 due to bright, persistent emissions from the sources.

Thus, there might be more superbursts or intermediate-duration bursts, which have not been noticed with the nova-alert system, in the MAXI data.

5.2.3 Stellar flares

The nova-alert system has often triggered on luminous X-ray stellar flares from various types of stars [dMe, dKe, RS CVn, Algol, Young Stellar Object (YSO), and other types of stars] in 1-scan or 4-orbit timescale bins (see tables 3, 8, and figure 7b).

X-ray flares from three RS CVns, GT Mus (= 4U 1137−65) (Nakajima et al. 2010), SZ Psc (Negoro et al. 2011c) and V841 Cen, and also from a YSO TWA-7 (Morii et al. 2010b; also see Uzawa et al. 2011), were detected for the first time (Tsuboi et al. 2014).

Tsuboi et al. (2014) collected 64 stellar flares from 22 stars, analyzing GSC images in the first four years, and found that the total energy of those flares was in the range of 10^{34} to 10^{39} erg, which was at the upper end for superflares.

We have reported on stellar flares to the ATel if they are historically the most luminous detected from a source, e.g., Eta Carinae reaching approximately 40 mCrab on 2014 July 15 and 17 (Negoro et al. 2014b), or if they are the first detection with MAXI, e.g., IM Peg triggered on 2014 July 5 (Kawagoe et al. 2014a) and July 16 (Kawagoe et al. 2014b). If they were neither, we have only circulated the events through the `X-ray-star` ML.

We note that fluxes of stellar flares are often around the detection limit in one scan transit (80–100 mCrab) or less. As a result, the detection of faint flares was incomplete for the data especially before the installation of the real-time background subtraction function in the nova-search system in 2011 March (subsection 4.2, also see Tsuboi et al. 2014).

[16] This number does not include bursts which are found to be non-GRB events later, e.g., GRB 121225A (sub-subsection 5.3.3), GRB 141029A, and occurred out of the FOVs, e.g., GRB 140219A (Serino et al. 2014b).

[17] The full burst list MAXI detected is available at ⟨http://maxi.riken.jp/grbs⟩.

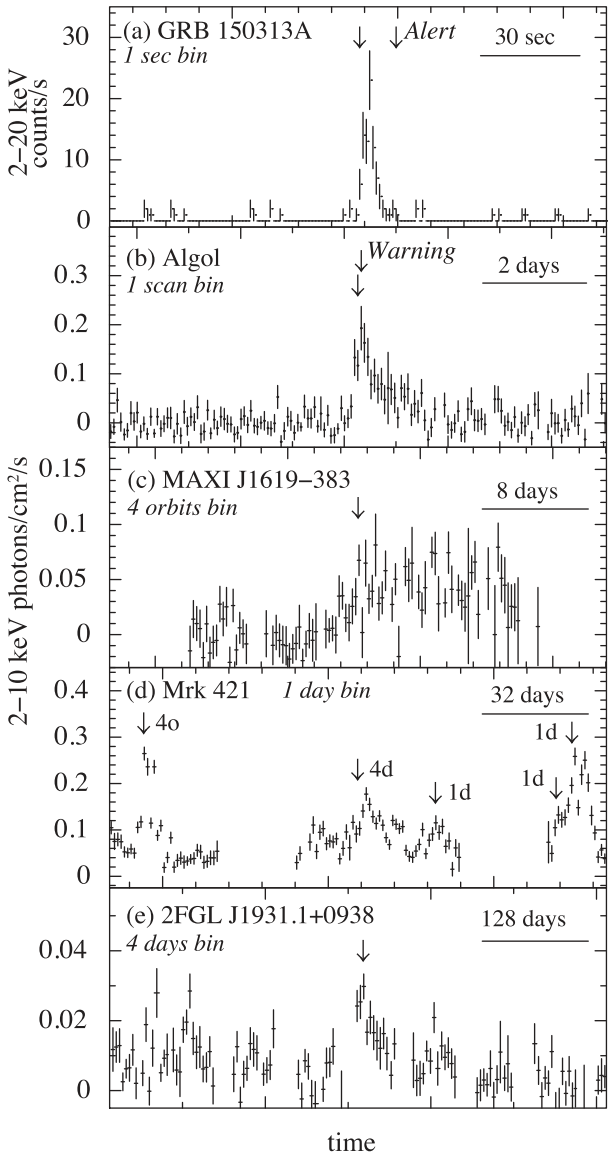

Fig. 7. Examples of light curves of transient events on various timescales, which triggered the nova-alert system. The arrows show the time when the nova-alert system was triggered, and the time when an alert e-mail has been issued is also shown in the panels (a) and (b). The data bin width is shown in each panel, and each curve has 150 data bins including no count or no observation period. From the upper to lower panels: (a) GRB 150313A (Morooka et al. 2015), (b) an X-ray flare from the eclipsing binary Beta Per (a.k.a. Algol) on 2012 December 17 (Nakahira et al. 2012), (c) an X-ray outburst of MAXI J1619−383 (Serino et al. 2014c), (d) multiple X-ray flares from the BL Lac Mrk 421 in 2013 [Negoro et al. (2013b) and Ueno et al. (2013)], where the trigger time bins are shown (4o = 4-orbit, 1d = 1 d, and 4 d = 4-d bins, respectively), and (e) an X-ray flare with about 10 mCrab of the BL Lac 2FGL J1931.1+0938 (Negoro et al. 2014a). The vertical axis units are 2–20 keV counts s^{-1} for panel (a) and 2–10 keV photons cm^{-2} s^{-1} for the others (b)–(e). 0.285 photons cm^{-2} s^{-1} corresponds approximately to 100 mCrab for (b)–(e). The start times of the curves are (a) 2015-03-13T03:50:49.077 (MJD 57094.16029024), (b) 2012-12-12T11:16 (MJD 56273.4700), (c) 2014-10-26T13:12 (MJD 56956.55), (d) 2013-04-02 (MJD 56384), and (e) 2013-04-30 (MJD 56412), respectively.

5.3 Newly discovered X-ray novae

In total 15 X-ray novae [six black hole candidates (BHCs), eight neutron star binaries, and one white dwarf binary] have been newly discovered with the nova-alert system, summarized in table 4. Figure 8 shows their long-term X-ray light curves. All the novae were automatically detected with the system, except for MAXI J1409−619, MAXI J1836−194, and MAXI J1647−227 (for references, see table 4), which were manually found in nova-search images before the automatic detection was running.

A few transients were independently discovered with Swift/BAT (e.g., Krimm et al. 2013b), having alternative names as listed in table 4 and described later.

As listed in table 4, most of the X-ray novae were discovered at a flux level of 30–40 mCrab, corresponding to a gradual increase in the X-ray flux on a timescale of hours (cf. table 1). The angular distances δr between the source locations reported on from MAXI and Swift/XRT observations indicate that the accuracy of the localization by MAXI is about 10′–20′ at that flux level (table 5). Due to the Sun angle constraint, however, no Swift/XRT observation was performed for MAXI J1619−383. Next we briefly summarize observational properties of the new transients, or introduce papers already published.

5.3.1 Six black hole candidates

Early detections of the BHCs and the prompt alerts to the world with the nova-alert system led rapid follow-up observations with Swift/XRT. With precise source locations given by XRT, other observatories could observe initial rising phases of the outbursts successfully, including the hard-to-soft state transitions, in multiple wavelengths.

The observational properties of six MAXI BHCs obtained by MAXI and follow-up observations are reviewed in Negoro and MAXI team (2014) and references therein. The six X-ray novae can be classified into two types of outbursts in terms of the long-term variations; a classical FRED (fast rise and exponential decay) type or a FRFT (fast rise and flat top) type. The former includes J1836−194, J1910−057, and J1828−249. The relationship between these different types of outbursts and state transitions, and the cause of the difference, are also briefly discussed in Negoro and MAXI team (2014).

5.3.2 X-ray pulsars and X-ray bursters

After the discovery of MAXI J1409−619, 503 ± 10 s pulsations were found in a Swift/XRT follow-up observation (Kennea et al. 2010b), and later a more precise pulse period of 506.93(5) s was obtained by Fermi/GBM monitoring (Camero-Arranz et al. 2010).

Table 4. New X-ray transients discovered by MAXI.

MAXI name	Detection			Type*	Alternate name†	Reference‡
	Trigger time (UT)§	Flux‖	Reference#			
J1659−152	10/09/25 08:36	30 ± 9	1	BHC	GRB 100925A[2]	21
J1409−619	(10/10/20)	41 ± 7	3	NS/Pulsar		
J0556−332	11/01/11 09:21	∼80	4	NS		22
J1543−564	11/05/08 04:21	21 ± 5	5	BHC		
J1836−194	(11/08/30)	∼25	6	BHC		
J0158−744	11/11/11 05:05	400(2–4 keV)	7	WD/SSS	XRF 111111A[7]	23
J1305−704	12/04/09 11:24	30 ± 18	8	BHC		24
J1910−057	12/05/31 22:36	38 ± 7	9	BHC	Swift J1910.2−0546[10]	25
J1647−227	(12/06/14)	33 ± 7	11	NS/XRB		26
(GRB 121225A)	12/12/25 09:50	500 ± 50	12	NS/XRB	Swift J1741.5−6548[13, 14]	
J1735−304	13/05/24 23:18	∼8	15	NS	Swift J1734.5−3027[16]	
J1828−249	13/10/15 21:55	93 ± 9	17	BHC		
J1421−613	14/01/09 01:13	40 ± 11	18	NS/XRB		27
J1932+091	14/05/26 18:09	∼40	19	SFXT?		
J1619−383	14/11/14 07:11	18 ± 3	20	NS/LMXB?		

*BHC = black hole candidate, NS = neutron star, XRB = X-ray burster, WD = white dwarf, SSS = super-soft source, SFXT = supergiant fast X-ray transient, LMXB = low-mass X-ray binary.

†‡References to the discoveries: [1] Negoro et al. (2010c), [2] Mangano et al. (2010), [3] Yamaoka et al. (2010), [4] Matsumura et al. (2011), [5] Negoro et al. (2011a), [6] Negoro et al. (2011b), [7] Kimura et al. (2011b), [8] Sato et al. (2012), [9] Usui et al. (2012), [10] Krimm et al. (2012), [11] Negoro et al. (2012a), [12] Ogawa et al. (2012), [13] Krimm et al. (2013a), [14] Negoro et al. (2013a), [15] Negoro et al. (2013c), [16] Kennea et al. (2013a), [17] Nakahira et al. (2013a), [18] Morooka et al. (2013), [19] Yamaoka et al. (2014), [20] Serino et al. (2014c).

‡References to detailed analysis results of MAXI observations: [21] Yamaoka et al. (2012), [22] Sugizaki et al. (2013), [23] Morii et al. (2013), [24] Morihana et al. (2013), Shidatsu et al. (2013), [25] Nakahira et al. (2014a), [26] Onodera et al. (2014), [27] Serino et al. (2015).

§Time in parentheses is not the trigger time, but the date when the source was found in nova-search images.

‖4–10 keV flux in units of mCrab reported on to the ATel.

Table 5. Localizations of MAXI X-ray transients.

MAXI name	RA (J2000.0)		Dec (J2000.0)		l	b	Error*	δr†	Ref.‡
	(°)		(°)		(°)	(°)			
J1659−152	254.75650	($16^h59^m01\overset{s}{.}71$)	−15.25848	(−15°15′28″.5)	5.515	16.526	1″.4	2′.1	1
J1409−619	212.01068	($14^h08^m02\overset{s}{.}56$)	−61.98340	(−61°59′00″.3)	311.797	−0.437	1″.9	7′.3	2
J0556−332	89.19300	($05^h56^h46\overset{s}{.}32$)	−33.17451	(−33°10′28″.2)	238.940	−25.183	1″.7	7′.0	3
J1543−564	235.822233	($15^h43^m17\overset{s}{.}336$)	−56.413431	(−56°24′48″.35)	325.085	−1.121	0″.6	1′.2	4
J1836−194	278.93097	($18^h35^m43\overset{s}{.}43$)	−19.32004	(−19°19′12″.1)	13.945	−5.354	1″.8	12′.0	5
J0158−744	29.85647	($01^h59^m25\overset{s}{.}55$)	−74.25795	(−74°15′28″.6)	296.801	−42.051	2″.4	10′.2	6
J1305−704	196.73138	($13^h06^m55\overset{s}{.}53$)	−70.45144	(−70°27′05″.2)	304.238	−7.619	2″.0	6′.7	7
J1910−057	287.59491	($19^h10^m22\overset{s}{.}78$)	−5.79943	(−05°47′58″.0)	29.902	−6.844	3″.5	4′.9	8
J1647−227	252.05134	($16^h48^m12\overset{s}{.}32$)	−23.01534	(−23°00′55″.2)	357.478	13.961	2″.4	16′.7	9
(GRB 121225A)	265.35051	($17^h41^m24\overset{s}{.}12$)	−65.79087	(−65°47′27″.1)	327.186	−17.823	1″.7	20′.6	(10)§
J1735−304	263.60074	($17^h34^m24\overset{s}{.}18$)	−30.39806	(−30°23′53″.0)	357.467	1.286	1″.4	13′.3	(11)§
J1828−249	277.24199	($18^h28^m58\overset{s}{.}08$)	−25.02925	(−25°01′45″.3)	8.115	−6.546	1″.9	10′.1	(12)§
J1421−613	215.40504	($14^h21^m37\overset{s}{.}21$)	−61.60700	(−61°36′25″.2)	313.438	−0.588	1″.5	15′.7	13
J1932+091	293.29267	($19^h33^m10\overset{s}{.}24$)	+9.19492	(+09°11′41″.7)	45.909	−4.947	2″.8	9′.6[14]	15
J1619−383	244.767	($16^h19^m04^s$)	−38.226	(−38°13′34″)	341.633	8.580	16′.8	N/A	16

*Positional error.

†Angular distance between the position reported to the ATel from the MAXI observations and that determined with Swift/XRT.

‡[1] Kennea et al. (2011b), [2] Kennea et al. (2010a), [3] Kennea et al. (2011a), [4] Chakrabarty, Jonker, and Markwardt (2010), [5] Kennea et al. (2011c), [6] Kennea et al. (2011d) [7] Kennea et al. (2012a), [8] Kennea et al. (2012b), [9] Kennea et al. (2012c), [10] Krimm et al. (2013a), [11] Kennea et al. (2013a), [12] Kennea et al. (2013b), [13] Kennea et al. (2014a), [14] Morii et al. (2014a), [15] Kennea et al. (2014c), [16] Morii et al. (2014b).

§In this paper, refined positions are shown.

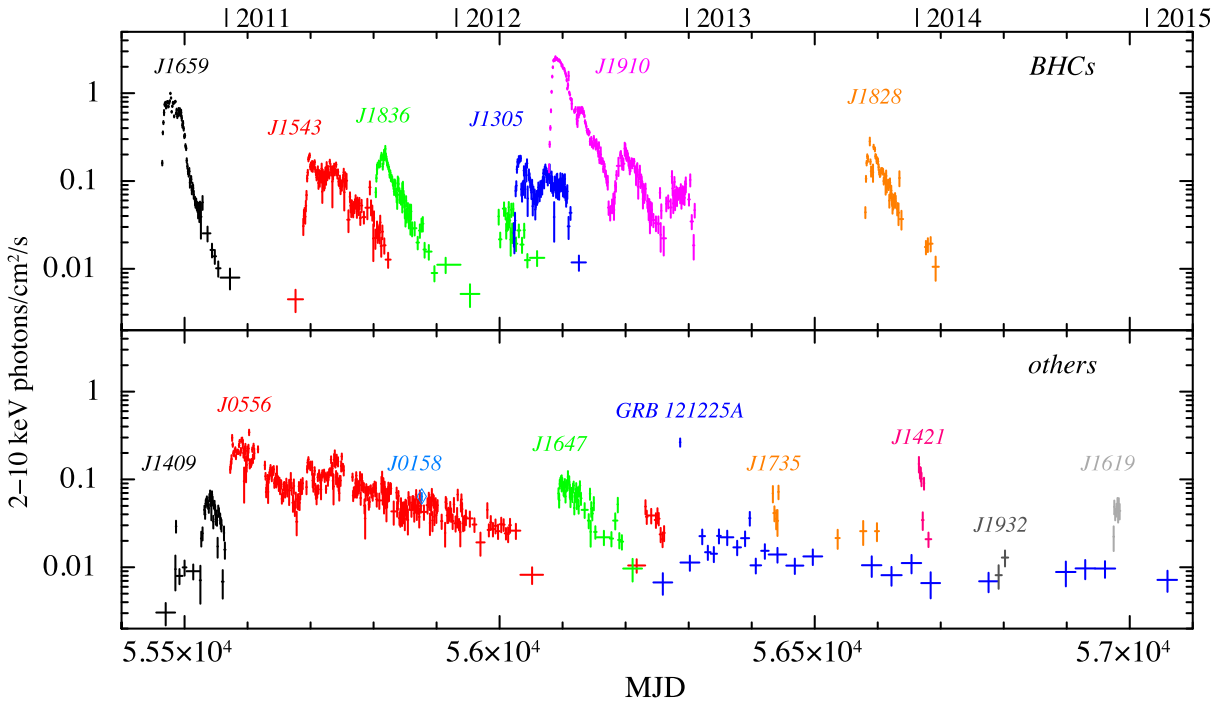

Fig. 8. 2–10 keV GSC light curves of black hole candidates (upper panel) and other transients (lower panel) newly discovered by MAXI. The curves are generated from 1 d public archival data at RIKEN, except for that of MAXI J1735−304 which was made with the on-demand analysis. For sources on the Galactic plane, the excess baseline counts due to the Galactic X-ray ridge emission were subtracted, being estimated from the data before or after the outbursts. Some data are rebinned using up to 30 d bins as the detection significance should be more than 5σ level if there is no time gap. Only more than 3σ detection data are shown. Note that 0.285 count s^{-1} cm^{-2} corresponds approximately to 100 mCrab. To avoid complexity, the curves have different colors (see color print or electric version), and MAXI J0158−744 is shown with the diamond mark.

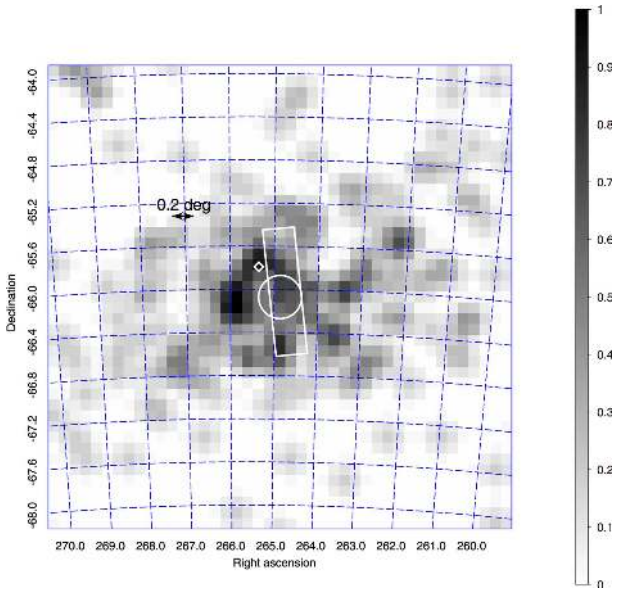

Fig. 9. X-ray image of GRB 121225A for one scan, obtained with GSC. The scanning time at the center of the image is 09:50 on 2012 December 25. The circular and the box regions show 90% confidence level error regions with and without the assumption of the constancy of the source flux, respectively. The small diamond indicates the position of Swift J1741.5−6548.

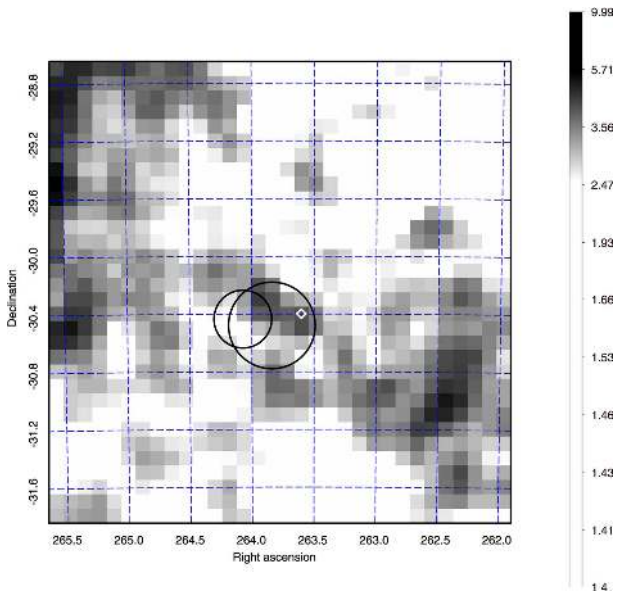

Fig. 10. X-ray image of MAXI J1735−304 obtained with GSC on 2013 May 24. The large error circle indicates an error region from MAXI observations. The small circle region represents the FOV of the Swift/XRT follow-up observation by Bahramian et al. (2013). The small diamond indicates the position of Swift J1734.5−3027.

Type-I X-ray bursts were detected from MAXI J1647−227 in a series of Swift follow-up observations (Kennea et al. 2012d) and MAXI J1421–613 during a Galactic plane scan survey with INTEGRAL/JEM-X (Bozzo et al. 2015).

A distant (>17 kpc), high Galactic latitude transient, MAXI J0556−332, exhibited a long outburst lasting for about 500 days, and the typical energy spectra of a low-mass X-ray binary hosting a neutron star, but no X-ray bursts were observed (Sugizaki et al. 2013). Interestingly, the source exhibited renewed activity about 180 days after a sudden drop of the flux (Sugizaki et al. 2012).

5.3.3 GRB 121225A (= Swift J1741.5−6548)

A burst-like event triggered the nova-alert system on 2012 December 25 (MJD 56286), and reported as GRB 121225A due to its relatively high galactic latitude ($l \simeq -17.^{\circ}8$). About three months later, Swift/BAT detected a faint X-ray enhancement, which was given the name Swift J1741.5−6548 (Krimm et al. 2013a).

The Swift position is, however, marginally consistent with that of GRB 121225A (figure 9), and the long-term light curve at the region showed a gradual increase after the burst (Negoro et al. 2013a). In figure 8, a faint (2–3 mCrab) enhancement can also be seen before the burst. The energy spectrum of the burst was also consistent with that of an X-ray burst to the distance of 10 kpc or less (Negoro et al. 2013a).

Optical spectroscopy with the Gemini Multi-Object Spectrograph (GMOS) supported the nature of Swift J1741.5−6548 to be a Galactic source (Cenko et al. 2013), and long-term hard X-ray activity using BAT data is also consistent with the above result as described in Krimm et al. (2013b). Thus, it is natural to consider that GRB 121225A is an X-ray burst at the beginning of the outburst of Swift J1741.5−6548, which is very similar to what was observed in M 15 X-2 (Morii et al. 2011; Tomida et al. 2013).

Finally, we note that a faint (∼3 mCrab) enhancement of the source was seen until the end of 2014 (figure 8).

5.3.4 MAXI J1735−304 (= Swift J1734.5−3027?)

On 2013 May 24 (MJD 56436), a faint X-ray enhancement toward the globular cluster Terzan 1 triggered the nova-alert system in 4-day time-bins, and we reported on a 4–10 keV source flux of about 8 mCrab, beginning on May 19 and lasting until at least June 1 (Negoro et al. 2013c). Renewed activity of XB 1732−304 or another source in the cluster was suspected, but no active source was found in the vicinity of the cluster in a single pointed observation with Swift/XRT (Bahramian et al. 2013; see figure 10).

On 2013 September 1, Swift/BAT caught burst-like activity from a source, newly named Swift J1734.5−3027, and the precise location was obtained with XRT (Kennea et al. 2013a). The position is $13.'3$ from MAXI J1735−304, and within the error circle of MAXI (figure 10). INTEGRAL/JEM-X also detected the source at the flux level of approximately 10 mCrab in the 3–10 keV band (Kuulkers et al. 2013). Using data from INTEGRAL, Swift, and XMM-Newton observations of the outburst, Bozzo et al. (2015) recently showed that the source was a neutron star at a distance of 7.2 ± 1.5 kpc.

La Parola et al. (2013) pointed out, utilizing BAT data at the position of Swift J1734.5−3027, that the source flux increased once from May 13 and peaked on May 30. In addition to the outburst in May (around MJD 56433–56443), the long-term GSC light curve (see figure 8) showed faint enhancements in September (around MJD 56533–56539), and October (around MJD 56572–56582 or –56602), which are very similar to the enhancements seen in the Swift/BAT light curve shown by Bozzo et al. (2015).

The extracted region to obtain the GSC light curve is relatively large ($65'$ radius) for a source-crowded region near the Galactic center, $(l, b) = (357.^{\circ}47, 1.^{\circ}29)$. Thus, careful analysis of the MAXI data was necessary. Nevertheless, MAXI J1735−304 and Swift J1734.5−3027 are thought to be identical, as far as the outbursts observed with Swift/BAT in May and September were from the same source.

Additionally, we note that an outburst-like activity starting from the end of 2010 November and lasting more than one month is recognized in the GSC light curve of the same region, but the origin of the outburst is unclear. Further discussion is, however, beyond the scope of this paper.

5.3.5 MAXI J1932+091

A short-lived, faint transient, MAXI J1932+091, triggered the nova-alert system on 2014 May 26 (MJD 56803). The source was detectable only for several hours for MAXI/GSC, but a Swift/XRT follow-up observation successfully caught a highly variable X-ray transient source with a 0.5–10 keV flux of $\sim 6 \times 10^{-11}$ erg cm^{-2} s^{-1} (Kennea et al. 2014c).

An initial possibility that the transient object was the BL Lac type AGN, 2FGL J1931.1+0938, lying near the error region was excluded from further MAXI data (Morii et al. 2014a). Instead, a strong Hα emission line and an Hβ line were observed in optical spectroscopic observations, suggesting that the source is a Be X-ray binary (Itoh et al. 2014). The short-lived, and highly variable, transient nature and a plausible supergiant companion suggest that the origin of the source is likely an SFXT (supergiant fast X-ray transient). The classification of the companion must make the nature of the source clear.

5.3.6 MAXI J1619−383

On 2014 November 14 (MJD 56975), the nova-alert system triggered on a faint X-ray transient with the flux near the 1 d detection limit (∼15 mCrab, figure 7c) at a relatively high Galactic latitude ($l \simeq 8.^{\circ}6$). However, it took a few days to confirm the presence of the source (Serino et al. 2014c).

Unfortunately, the source was close to the Sun (17–24°), and therefore other observatories were unable to observe the source. Two ROSAT bright sources, 1RXS J161838.4−381911 and 1RXS J161815.1−382027, are located within the error region, but the nature of the ROSAT sources are unknown.

The outburst with the peak flux of ∼20 mCrab lasted more than 10 days, and no spectral evolution was recognized. The energy spectrum can be fitted with a power-law model of the photon index of $1.43^{+0.43}_{-0.21}$ (Morii et al. 2014b). The count ratio of the 4–10 keV band to the 2–4 keV band is close to 1, which is a typical value of GSC spectra of BHCs in the intermediate state or neutron-star LMXBs (low-mass X-ray binaries). No X-ray burst was observed; however, the stability of the spectrum through the outburst suggests that the source is likely an LMXB hosting a neutron star.

5.3.7 MAXI J0158−744

A very bright, unusually soft X-ray nova (burst-like activity) was detected near the Small Magellanic Cloud, mostly in time bins in the 2–4 keV energy band, and the appearance was automatically circulated to the `New-transient` ML 55 s after the trigger time, 05:05:50 on 2011 November 11 (MJD 55876.21239) (Kimura et al. 2011b).[18]

By successful Swift/XRT follow-up observations (e.g., Kennea et al. 2011d), the source was soon found to be a supersoft source, SSS (Li et al. 2011). Morii et al. (2013) concluded that MAXI detected the ignition phase of a nova. For the first time, such a phenomenon was observed in X-rays (see also Ohtani et al. 2014).

5.4 Outbursts of known X-ray sources

We report on several new (type-II) outbursts (or renewed activities) from known BH or NS X-ray binaries every year (see tables 6–7). These numbers are roughly half of all the outbursts reported in the period. Except for 4U 1630−47, H 1743−322, 4U 1608−522, and Cir X-1 all showing an outburst almost every year, it is interesting to note that the number of known sources showing renewed activity is comparable to that of the new transients that appeared.

The nova-alert system has frequently triggered on (type-I/regular) outbursts associated with orbital periods from Be or other types of pulsars. We have not reported on the triggers of the nova-alert system by regular outbursters Cen X-3, Her X-1, Vela X-1, GX 301−4, and EXO 2030+375, but did for three semiregular Be pulsars, GX 304−1 (e.g., Nakajima et al. 2013), GRO J1008−57 (Nakajima et al. 2014a), and A0535+26 (Nakajima et al. 2014b), because of the interest in their long-term activities. In addition, unexpected irregular (type-II) outbursts that triggered the system were all reported, e.g., from GRO J1008−57 (Nakajima et al. 2014c).

We note that Suzaku Target of Opportunity (ToO) observations triggered by the MAXI alerts have led to the discovery of cyclotron absorption lines in energy spectra of GX 304−1 (Yamamoto et al. 2011) and GRO J1008−57 (Yamamoto et al. 2014).

5.5 State transitions of X-ray binaries

The nova-alert system does not implement an auto-detection algorithm to detect a state transition. As described in subsection 4.1, however, in addition to the function of the real-time X-ray transient monitor of the nova-search system, it regularly provides color scan-by-scan and daily all-sky images, which allow us to find the state transition of a source easily.

Examples: the hard-to-soft state transition after a long hard-state period in Cyg X-1 (Negoro et al. 2010b); the discovery of a short-lived soft state in Swift J1753.5−0127 (Negoro et al. 2009, also see Yoshikawa et al. 2015); the first detection of the transition to the soft state in the LMXB GS 1826−238 (Nakahira et al. 2014c) are worth noting.

5.6 AGN flares and tidal disruption events

5.6.1 AGN flares

Almost every year, the nova-alert system triggers on flares from bright AGNs, 3C 273, NGC 5506, Mrk 421, and Mrk 501 in long timescale bins (1-scan to 4 d time bins). We usually call attention to the events through the `AGN` ML.

The system successfully was triggered by the beginning of a very bright (and long) flare of Mrk 501 with a flux of ∼10 mCrab on 2011 November 9 (Sootome et al. 2011; and two months later, reaching a peak flux of ∼20 mCrab), and the historically brightest flares of Mrk 421 (see figure 7d) on 2010 February 12 (156 ± 11 mCrab at 2–10 keV on February 16, Isobe et al. 2010a; see also Isobe et al. 2010b for more detail), on 2013 April 12–15 (∼140 mCrab on April 12, Negoro et al. 2013b), and on 2013 August 14–23 (∼80 mCrab on August 20, Ueno et al. 2013; also Isobe et al. 2015).

The nova-alert system also caught historically bright flares from three BL Lac objects around the detection limit

[18] The time 05:05:59 in the ATel report was not the trigger time, but the time that the highest significant detection was achieved.

(7–8 mCrab for 4 d): 1ES 0033+595 (QSO B0033+595) on 2013 February and March (Kawamuro et al. 2013); 2FGL J1931.1+0938 (BZB J1931+0937) on 2014 March 2 (Negoro et al. 2014a; Kennea et al. 2014b; figure 7e); and BZB J0244−5819 on 2014 March 24 (Nakahira et al. 2014b).

5.6.2 Swift J164449.3+573451

A highly variable tidal disruption event (Burrows et al. 2011; Zauderer et al. 2011), Swift J164449.3+573451, was first reported from a Swift/BAT observation on 2011 March 28 (Cummings et al. 2011). The source in exhibiting the first bright flare that triggered BAT at 12:57 was out of the FOVs of MAXI/GSC. Soon after the BAT report to the GCN circular, however, it was found that GSC marginally detected faint activities before the first bright flare in the scan transits at 10:31 (44 ± 22 mCrab) and at 12:03 (77 ± 28 mCrab) (Kimura et al. 2011a). Source activity starting about 3.5 d before BAT was first triggered (Burrows et al. 2011) was not significantly detected with GSC.

However, about 31 hours after BAT was first triggered, the nova-alert system was triggered by a second intense flare from the source in various time bins, from 3 s to 1 d, at 20:07:58 on 2011 March 29, and the event was immediately circulated through the AGN ML.

6 Discussion and summary

We demonstrate in this paper that MAXI has detected a number of transient events with the MAXI nova-alert system, and played an important role in the search for the transient events in the soft X-ray band after RXTE/ASM. MAXI complementarily works with the hard X-ray monitors of Swift/BAT, INTEGRAL/IBIS, and Fermi/GBM to discover various transient objects.

A relatively large number of the new galactic transient objects discovered at high galactic latitude, for instance MAXI J1659−152, MAXI J0556−332, MAXI J1647−227, and Swift J1741.5−6548 (GRB 121225A), are worth noting from a statistical point of view in the binary formation theory, because a number of main-sequence stars and most X-ray binaries with persistent emission are on or near the galactic plane. It might be, however, due to a selection effect, because it is more difficult to find new transients at low Galactic latitude due to source confusion and higher backgrounds. More detailed discussion including the nature of the sources will be reported elsewhere.

The nova-alert system is found to be helpful not only for the search for new transients, but also for the detection of spectral changes, such as state transitions of known X-ray binaries, as in the cases of in Cyg X-1 and Swift J1753.5−0127.

MAXI, with the highest sensitivity to date, and the nova-alert system have opened new windows upon luminous stellar flares described in sub-subsection 5.2.3 and a new class of soft X-ray transients, MAXI J0158−744, both of which were only detectable by MAXI.

Fast discovery of new transients with the nova-alert system and its prompt alerts has led to successful follow-up observations with Swift/XRT, not only for GRBs but also for X-ray transients such as MAXI J0158−744 and MAXI J1932+091. Thus, collaboration with other X-ray satellites, especially Swift/XRT which can perform a prompt follow-up observation to locate the transient with accuracy of nearly one arcsecond, is very important for MAXI.

As described in section 4, the system has been developed year by year and tuned according to changes in the observational conditions. The system and its detection parameters have already been optimized, so it is worth reanalyzing the data accrued since the beginning of the mission. Such a system is under development. The transient search using SSC data recently commenced in 2015 April (see Fukushima et al. 2014; Fukushima 2015).

Reanalysis with a new nova-alert system under development has shown that some tidal disruption events that occurred from 2009 to 2013 were detectable with the newly introduced 16- and/or 32-day time-bins, suggesting that in future tidal disruption events would be detected with the nova-alert system in real-time.

However, due to the relatively poor spatial resolution of the MAXI cameras, it is difficult for the current system to detect transients near bright objects, especially near the Galactic center and on the Galactic ridge. Multiple source image fits, for instance just like the RXTE Galactic Center Observation,[19] are necessary. This is planned for future work.

Acknowledgments

We thank Kazuhiro Hotta and Hiroyuki Nakamoto at Systems Engineering Consultants Co., Ltd. for the development and continuous support to maintain the MAXI-DB and its operation. We also thank laboratory members at Nihon University who made significant contributions to the development of parts of the MAXI nova-alert system; Ryoji Ishiwata to the alert system, Rie Goto to an auto-afterglow-search program for GRBs circulated in the GCN, Ryo Sasaki and Naoki Yamashita to a web interface ("masiv") of images produced by the nova-search system, Shintaro Yoshida and Yuutaro Ishikawa to an auto-catalogue-update program, and Naoto Tanabe to the MAXI database. Finally, we thank all the MAXI team members for paying close attention to transient events that triggered the nova-alert system.

[19] ⟨http://asd.gsfc.nasa.gov/Craig.Markwardt//galscan/main.html⟩.

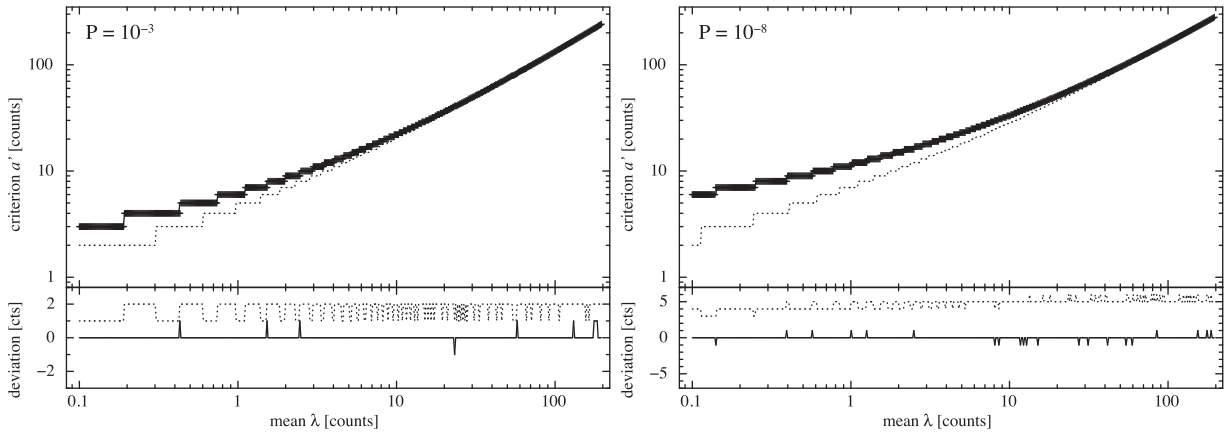

Fig. 11. Criteria for various means, λ, and given possibilities, $P = 10^{-3}$ (left) and $P = 10^{-8}$ (right), calculated from the Poisson distribution (solid), the normal distribution (dotted), and the approximate formula (marks "+", which are mostly on the solid line.). Their deviations from the criteria based on the Poisson distributions are also shown by the solid lines in the lower panels (see text).

This work was supported by JSPS KAKENHI Grant Numbers 21340043, 23540269, 24540239, and also by JAXA. Some of the results in this paper have been derived using the HEALPix (Górski et al. 2005) package.

Appendix 1. Method of the fast calculation of the criterion

Here, we describe an approximation formula to obtain a criterion for the number of counts a to detect a significant count increase in the light curve.

Based on Poisson statistics for a mean number of counts λ, and a given chance probability P that the (observed) number of counts r equals or exceeds a, the criterion a should be the minimum number satisfying the following equation:

$$P \geq P_\lambda(r \geq a) \equiv 1 - \sum_{r=0}^{a-1} \frac{\lambda^r e^{-\lambda}}{r!} = 1 - \frac{\Gamma(a,\lambda)}{\Gamma(a)} = \frac{\gamma(a,\lambda)}{\Gamma(a)}, \quad \text{(A1)}$$

where $\Gamma(a)$ is the gamma function with a positive integer a, and $\Gamma(a, \lambda)$ and $\gamma(a, \lambda)$ are the upper and the lower incomplete gamma functions, respectively.

In practical data, λ takes from $\sim$0.1 to $\sim$200 [counts bin^{-1}], and the above exact formula needs a number of calculations, especially for large λ. This makes it difficult to obtain about 10^3 ($\sim$100 pixels s^{-1} $\times$ 8 time-series bins) criteria in each second. To reduce the calculation time greatly, we introduce an approximate function to obtain a simply by assigning λ and P.

For $\lambda < 1$,

$$P_\lambda(r \geq a) = \frac{1}{(a-1)!}\int_0^\lambda e^{-t} t^{a-1} dt \simeq \frac{\alpha}{a!} e^{-\lambda}\lambda^a, \quad \text{(A2)}$$

where α is a constant close to unity. This formula gives better approximations for larger numbers of a, for instance $a > 7$, used practically.

From the above and the Stirling's approximations, we obtain

$$a \simeq -\frac{\ln P_\lambda - \ln\alpha + \lambda + O(\ln a)}{\ln(a/\lambda) - 1} \sim -\beta \ln P_\lambda (= -\ln P_\lambda \lambda^{\ln\beta/\ln\lambda}), \quad \text{(A3)}$$

where

$$\beta(P_\lambda, \lambda) = \{\ln(a/\lambda) - 1\}^{-1}.$$

β weakly depends on P_λ and λ, and is $0.3 \sim 0.8$ for $\lambda < 1$ and $P_\lambda = 10^{-3} \sim 10^{-8}$.

On the other hand, for $\lambda \gg 1$, it is known that the Poisson distribution is close to the normal distribution with mean λ and variance λ. Thus, using the inverse complementary error function, erfc$^{-1}(P)$,[20] a is expected to be written as

$$a(P, \lambda) = \lambda + \sqrt{2\lambda}\,\mathrm{erfc}^{-1}(2P). \quad \text{(A4)}$$

Note that P here is not P_λ, and a is no longer an integer.

From equations (A3) and (A4), a for a wide range of λ may be approximately expressed as

$$a(P, \lambda) = \lambda + \sqrt{\lambda}\{c_0(P)\lambda^{c_1(P)} + \sqrt{2}\mathrm{erfc}^{-1}(2P) + c_2(P)\}, \quad \text{(A5)}$$

[20] In fact, the numerical function *dierfc* by T. Ooura is used: ⟨http://www.kurims.kyoto-u.ac.jp/~ooura/gamerf.html⟩.

Table 6. ATel reports summary of galactic black hole candidates.

Type	Phenomena	Object name	ATel number (year/month)
Black hole candidate	Outburst	4U 1630−47	2363 (09/12), 3830 (11/12), 4992 (13/04), 6991 (15/01)
		H 1743−322	2364 (09/12), 2774 (10/08), 3842 (12/01), 4419 (12/09), 5241 (13/08)
		GX 339−4	2380 (10/01)
		MAXI J1659−152	2873 (10/09)
		SLX 1746−331	3098 (11/01)
		MAXI J1543−564	3330 (11/05)
		MAXI J1836−194	3611 (11/08)
		MAXI J1305−704	4024 (12/04)
		MAXI J1910−057	4140 (12/06)
		MAXI J1828−249	5474 (13/10)
		V4641 Sgr	5803 (14/01)
		XTE J1856+053	7233 (15/03)
	State transition	Swift J1753.5−0127	2341 (09/12), 7196 (15/03)
		H 1743−322	2378 (10/01)
		XTE J1752−223	2396 (10/01)
		Cyg X-3†	2404 (10/01), 2635 (10/05), 3139 (11/02)
		Cyg X-1	2711 (10/07), 3534 (11/08), 6115 (14/05)
		MAXI J1836−194	3626 (11/09)
		MAXI J1305−704	4035 (12/04)
		4U 1630−47	4075 (12/04), 4395* (12/09), 4406 (12/09)
		MAXI J1910−057	4198 (12/06), 4273 (12/07)
		MAXI J1828−249	5483 (13/10)
		XTE J1908+094	5549 (13/11)
	(Brightening)	XTE J1752−223	2259 (09/10)

*Reports by other than MAXI team members.
†Cyg X-3 is tentatively classified as a black hole candidate here.

Table 7. ATel reports summary of neutron stars.

Type	Phenomena	Object name	ATel number (year/month)
LMXB (NS)	Outburst	SAX J1748.9−2021 in NGC 6440	2360 (09/12)
		4U 1711−34	2425 (10/02)
		4U 1608−522	2462 (10/03), 3237 (11/03), 4478 (12/10), 6550 (14/10)
		Cir X-1	2608 (10/05), 2674 (10/06), 4661 (12/12)
		XTE J1709−267	2729 (10/07), 5319 (13/08)
		MAXI J0556−332	3102 (11/01)
		SAX J1747.0–2853	3123 (11/01), 5041 (13/05)
		Swift J1922.7−1716	3548 (11/08)
		IGR J17191−2821	4170 (12/06)
		MAXI J1647−227	4175 (12/06)
		XTE J1810−189	4752 (13/01)
		MAXI J1735−304	5096 (13/06)
		1A 1744−361 in NGC 6441	5301* (13/08)
		M 15 X-2	5327 (13/08)
		MAXI J1421−613	5750 (14/01)
		Aql X-1	7088 (15/02)

Table 7. (Continued)

Type	Phenomena	Object name	ATel number (year/month)
	State transition	Swift J1922.7−1716	3807 (11/12)
		4U 1608−522	5094* (13/05)
		GS 1826−238	6250 (14/06)
	X-ray burst	M 15 X-2	3356 (11/05)
		1A 1246−588	3482 (11/07)
		IGR J18245−2452 in M 28	4961 (13/04)
	Superburst	4U 1820−30	3625* (11/09)
		EXO 1745−248 in Terzan 5	3729 (11/11)
		SAX J1828.5−1037†	3760 (11/11)
		SLX 1735−269†	4622 (12/12)
		4U 1850−08	5978 (14/03)
		4U 0614+091	6668 (14/11)
	(Brightening)	4U 2206+54	2271 (09/10)
		4U 1323−619	2399 (10/01)
		4U 1954+319	2702 (10/06)
		MAXI J0556−332	4524 (12/10)
		GRB 121225A	4911 (13/03)
		4U 1700+24	6850 (14/12)
		1RXS J180408.9−342058	7008 (15/01)
	(flux drop)	GX 13+1	6433 (14/09)
Pulsar	Outburst	A 0535+26	2277 (09/10), 2754 (10/07), 2970 (10/10), 5931 (14/02), 6569 (14/10), 7015 (15/02)
		GX 304−1	2297 (09/11), 2779 (10/08), 3075 (10/12), 3309 (11/04), 3624 (11/09), 3856 (12/01), 4420 (12/09), 5205 (13/07)
		V 0332+53	2369 (10/01), 2427 (10/02)
		LS V +44 17	2527 (10/03)
		GRO J1008−57	2769 (10/08), 3796 (11/12), 4355* (12/09), 4561 (12/11), 5004* (13/04), 5705 (13/12), 6465 (14/09), 6630(14/10), 6656* (14/11), 6819 (14/12), 6917* (15/01)
		MAXI J1409−619	2959 (10/10)
		XTE J1946+274	3048 (10/11)
		4U 0115+63	3430 (11/06), 3677 (11/10)
		4U 0142+61	3530 (11/08)
		XTE J1858+034	3766 (11/11)
		4U 1901+03	3829 (11/12)
		KS 1947+300	5438 (13/10)
		GRO J1744−28	5790 (14/01)
		Cep X-4	6212 (14/06)
		2S 1553−542	7018 (15/02)
		XTE J1859+083	7034 (15/02)
		H 1145−619	7215 (15/03)
	(Brightening)	MAXI J1409−619	3067 (10/12)
		Swift J1843.5−0343	3114 (11/01)
		GRO J1744−28	5963 (14/03)
SFXT	Outburst(flare)	AX J1841.0−0536	3018 (10/11)
		XTE J1739−302†	6900 (15/01)

*Telegrams by other than MAXI team members.

†The most probable candidate in crowed region, not confirmed by any other observatory.

Table 8. ATel reports summary of active stars, AGNs, and others.

Type	Sub-class or phenomena	Object name	ATel number (year/month)
Star	dMe/dKe	EQ Peg	3107 (11/01)
		YZ CMi	3211 (11/03)
		CC Eri	3837 (11/12)
		V1054 Oph	4114 (12/05)
		UV Ceti	4671 (12/12), 6026 (14/03)
		AT Mic	5661 (13/12)
		BY Dra*	6042 (14/04)
		FK Aqr	6120 (14/05)
	RS CVn	HR 1099	2401 (10/01)
		GT Mus	3021 (10/11)
		UX Ari	3308 (11/04), 6315 (14/07)
		SZ Psc	3737 (11/11)
		CF Tuc	3897 (12/01)
		IM Peg	6296 (14/07), 6322 (14/07)
		Sigma Gem	6817 (14/12)
		V824 Ara	6908 (15/01)
	Algol	Algol	3096 (10/12), 3809 (11/12), 4656 (12/12), 4841 (13/02)
	YSO	TWA-7	2836 (10/09)
	Others	HD 347929	2700 (10/06), 5075 (13/05)
		Eta Car	6289 (14/07)
		1RXS J043657.1−161258	6654(14/11)
LMC	WD/Nova	MAXI J0158−744	3756 (11/11)
& SMC	Pulsar/outburst	Swift J0549.7−6812	5289 (13/08)
	Unknown/outburst	MAXI J0057−720†	5925 (14/02)
AGN	Tidal disruption	Swift J164449.3+573451	3244 (11/03)
	BL Lac/flare	Mrk 421	2368 (10/01), 2444 (10/02), 3637 (11/09), 4978 (13/04), 5320 (13/08)
		Mrk 501	3752 (11/11)
		1ES 0033+595	4877 (13/03)
		2FGL J1931.1+0938	5943 (14/03)
		BZB J0244−5819	6012 (14/03)
GRB	Prompt emission	GRB 111215A	3810 (11/12)
Unknown	Short burst	(No name)	2321 (09/12), 2415 (10/02), 2476 (10/03), 2524 (10/03), 2842 (10/09), 2990 (10/10)
		MAXI J1631−639	3316 (11/04)
		MAXI J0827+811‡	5444 (13/10)
		MAXI J0545+043	6066 (14/04)
		MAXI J0511−522	7200 (15/03)
	Outburst?	MAXI J1807−228†	4335 (12/08)
		MAXI J1932+091	6174 (14/05), 6184 (14/05)
		MAXI J1619−383	6708 (14/11), 6767 (14/11)

*Not significantly detected.
†MAXI J0057–720 and MAXI J1807−228 might be identical to AX J0058–720 and SAX J1806.5−2215, respectively.
‡V496 Cam is within the error region of MAXI J0827+811, but not confirmed.

where

$$c_0(P) = -\ln P, \quad c_1(P) = \frac{\ln \beta}{\ln \lambda} - \frac{1}{2}. \tag{A6}$$

The additional term $c_2(P)$ is introduced for a better approximation described later.

Furthermore, recalling β to be weakly dependent on P_λ, we replace all c_i by

$$c_i = c_{il} \log_{10} P + c_{ic}, (i = 0, 1, 2),$$

where c_{il} and c_{ic} are constants, and we obtain the following values from fits to proper curves calculated from the lower

incomplete gamma function γ/Γ in equation (A1) for $0.1 \leq \lambda \leq 200$ and $10^{-9} \leq P \leq 10^{-2.5}$:

$$c_0(P) = -0.5673 \log_{10} P - 0.0442, \quad \text{(A7)}$$

$$c_1(P) = -0.00314 \log_{10} P - 0.4406, \quad \text{(A8)}$$

$$c_2(P) = 0.0177 \log_{10} P + 0.0087. \quad \text{(A9)}$$

c_0 is dominated by the log coefficient c_{0l} as expected from equation (A6). The other parameters are all small, but we confirm that those are necessary to give better fits.

Figure 11 shows examples of the criteria for $P = 10^{-3}$ (left) and $P = 10^{-8}$ (right) for various λ obtained from the Poisson distribution [equation (A1), solid lines in the upper panels] and the approximate function [equation (A5), marks] using parameters in equations (A7)–(A9). The actual criteria a' are $\lceil a \rceil$, where $\lceil \ldots \rceil$ is the ceiling function and the value of a is that of equation (A5). The normal distribution cases [equation (A4), and $a' = \lceil a \rceil$] are also shown by the dotted lines.

The solid lines in the lower panels of both the figures show the deviations of the approximate solutions from the exact ones. Values λ are logarithmically sampled; only 10 and 21 data points in 510 show difference by 1 count, which can be negligible for our purpose. Finally, it is interesting to note that the contribution of $c_0\lambda^{c_1}$ to the total count is significant for smaller λ, and almost constant $\sim 0.5 \log_{10} P$ through all λ as is expected in equations (A5), (A7), and (A8), shown by the dotted lines in the lower panels.

Appendix 2. Transient events reported to the Astronomer's Telegram

Here we list transient events reported to the Astronomer's Telegram, in tables 6–8. The list includes telegrams written not only by the MAXI team members, but also by others when the events were reported as a result of substantially using MAXI data (marked with "*" in the tables).

We also note that tables 6–8 include several transient activities recognized not by the nova-alert system, but by light curves of individual objects, or detections with Swift/BAT or Fermi/GBM, e.g., A 0535+26 (Sugizaki et al. 2009), mainly in ATel reports posted in 2009, when the nova-alert system had not fully worked.

References

Asada, M., et al. 2011, Astronomer's Telegram, 3760

Bahramian, A., Heinke, C. O., Sivakoff, G. R., Wijnands, R., Altamirano, D., Homan, J., Pooley, D., & Gladstone, J. C. 2013, Astronomer's Telegram, 5116

Bozzo, E., et al. 2014, Astronomer's Telegram, 5765

Bozzo, E., Romano, P., Falanga, M., Ferrigno, C., Papitto, A., & Krimm, H. A. 2015, A&A, 579, 56

Burrows, D.N., et al. 2011, Nature, 476, 421

Camero-Arranz, A., Finger, M. H., & Jenke, P. 2010, Astronomer's Telegram, 3069

Case, G. L., et al. 2011, ApJ, 729, 105

Cenko, S. B., Greiner, J., & Krimm, H. A. 2013, Astronomer's Telegram, 4919

Chakrabarty, D., Jonker, P.G., & Markwardt, C. B. 2011, Astronomer's Telegram, 3407

Chenevez, J., et al. 2011, Astronomer's Telegram, 3183

Cummings, J. R., et al. 2011, GCN Circ., 11823

Fukushima, K. 2015, Master's thesis, Nihon University

Fukushima, K., et al. 2014, in Proc. Suzaku-MAXI 2014: Expanding the Frontiers of the X-ray Universe, ed. M. Ishida et al. (Ehime: Ehime University), 146

Fukushima, K., et al. 2015, GCN Circ., 17345

Galloway, D. K., Muno, M. P., Hartman, J. M., Psaltis, D., & Chakrabarty, D. 2008, ApJS, 179, 360

Gehrels, N., et al. 2004, ApJ, 611, 1005

Górski, K. M., Hivon, E., Banday, A. J., Wandelt, B. D., Hansen, F. K., Reinecke, M., & Bartelmann, M. 2005, ApJ, 622, 759

Heinke, C. O., Sivakoff, G. R., Morii, M., & Kuulkers, E. 2011, Astronomer's Telegram, 3363

Honda, F., et al. 2014, GCN Circ. 16702

in't Zand, J. 2011, in Proc. 4th International MAXI Workshop, The First Year of MAXI: Monitoring Variable X-ray Sources, ed. T. Mihara & M. Serino (Sagamihara: Aoyama Gakuin University), 169

in't Zand, J., Serino, M., Kawai, N., & Heinke, C. 2011, Astronomer's Telegram, 3625

Ishikawa, M., et al. 2009, in Proc. 3rd International MAXI Workshop, Astrophysics with All-Sky X-ray Observations, ed. N. Kawai et al. JAXA-SP-08-014E (Chofu, Tokyo: JAXA), 30

Isobe, N., et al. 2010a, Astronomer's Telegram, 2444

Isobe, N., et al. 2010b, PASJ, 62, L55

Isobe, N., et al. 2015, ApJ, 798, 27

Itoh, R., et al. 2014, Astronomer's Telegram, 6186

Kawagoe, A., et al. 2014a, Astronomer's Telegram, 6296

Kawagoe, A., et al. 2014b, Astronomer's Telegram, 6322

Kawamuro, T., et al. 2013, Astronomer's Telegram, 4877

Kennea, J. A., et al. 2011b, ApJ, 736, 22

Kennea, J. A., et al. 2011c, Astronomer's Telegram, 3613

Kennea, J. A., et al. 2011d, Astronomer's Telegram, 3758

Kennea, J. A., et al. 2012a, Astronomer's Telegram, 4034

Kennea, J. A., et al. 2012b, Astronomer's Telegram, 4145

Kennea, J. A., et al. 2012d, Astronomer's Telegram, 4192

Kennea, J. A., et al. 2013a, Astronomer's Telegram, 5354

Kennea, J. A., et al. 2013b, Astronomer's Telegram, 5478

Kennea, J. A., et al. 2014c, Astronomer's Telegram, 6177

Kennea, J. A., Curran, P., Krimm, H., Romano, P., Mangano, V., Evans, P. A., Yamaoka, K., & Burrows, D. N. 2010b, Astronomer's Telegram, 3060

Kennea, J. A., Evans, P., Krimm, H., Romano, P., Mangano, V., Curran, P., & Yamaoka, K. 2011a, Astronomer's Telegram, 3103

Kennea, J. A., Evans, P. A., Krimm, H. A., Romano, P., Mangano, V., Curran, P., Yamaoka, K., & Negoro, H. 2012c, Astronomer's Telegram, 4178
Kennea, J. A., Krimm, H. A., Evans, P. A., Romano, P., Mangano, V., Curran, P., Yamaoka, K., & Negoro, H. 2014a, Astronomer's Telegram, 5780
Kennea, J. A., Krimm, H. A., Evans, P. A., Romano, P., Mangano, V., Curran, P., Yamaoka, K., & Negoro, H. 2014b, Astronomer's Telegram, 5946
Kennea, J. A., Krimm, H., Romano, P., Mangano, V., Curran, P., & Evans, P. 2010a, Astronomer's Telegram, 2962
Kimura, M., et al. 2011a, Astronomer's Telegram, 3244
Kimura, M., et al. 2011b, Astronomer's Telegram, 3756
Krimm, H. A., et al. 2012, Astronomer's Telegram, 4139
Krimm, H. A., et al. 2013a, Astronomer's Telegram, 4902
Krimm, H. A., et al. 2013b, ApJS, 209, 14
Kuulkers, E., et al. 2013, Astronomer's Telegram, 5361
La Parola, V., Segreto, A., Cusumano, G., & Maselli, A. 2013, Astronomer's Telegram, 5646
Levine, A. M., Bradt, H., Cui, W., Jernigan, J. G., Morgan, E. H., Remillard, R., Shirey, R. E., & Smith, D. A. 1996, ApJ, 469, L33
Lund, N., et al. 2003, A&A, 411, L231
Li, K. L., Kong, A. K. H., Tam, P. H. T., & Wu, J. H. K. 2011, Astronomer's Telegram, 3759
Mangano, V., Hoversten, E. A., Markwardt, C. B., Sbarufatti, B., Starling, R. L. C., & Ukwatta, T. N., 2010, GCN Circ., 11296
Matsuoka, M., et al. 2009a, PASJ, 61, 999 (M09)
Matsuoka, M., et al. 2009b, GCN Circ., 9852
Matsumura, T., et al. 2011, Astronomer's Telegram, 3102
Meegan, C., et al. 2009, ApJ, 702, 791
Mereghetti, S., Götz, D., Borkowski, J., Walter, R., & Pedersen, H. 2003, A&A, 411, L291
Mihara, T., et al. 2011a, PASJ, 63, S623
Mihara, T., et al. 2011b, Astronomer's Telegram, 3729
Miller-Jones, J. C. A., Sivakoff, G. R., Heinke, C. O., Altamirano, D., Kuulkers, E., & Morii, M. 2011, Astronomer's Telegram, 3378
Miyoshi, S. 2010, Master's thesis, Nihon University
Morihana, K., et al. 2013, PASJ, 65, L10
Morii, M., et al. 2010a, in AIP Conf. Proc., 1279, Deciphering the Ancient Universe with Gamma-Ray Bursts, ed. N. Kawai & S. Nagataki (New York: AIP), 391
Morii, M., et al. 2010b, Astronomer's Telegram, 2836
Morii, M., et al. 2011, Astronomer's Telegram, 3356
Morii, M., et al. 2013, ApJ, 779, 118
Morii, M., et al. 2014a, Astronomer's Telegram, 6184
Morii, M., et al. 2014b, Astronomer's Telegram, 6767
Morii, M., Yamaoka, H., Mihara, T., Matsuoka, M., & Kawai, N. 2016, PASJ, 68, S11
Morooka, Y., et al. 2013, Astronomer's Telegram, 5750
Morooka, Y., et al. 2015, GCN Circ. 17572
Nakahira, S., et al. 2012, Astronomer's Telegram, 4656
Nakahira, S., et al. 2013a, Astronomer's Telegram, 5474
Nakahira, S., et al. 2013b, J. Space Sci. Info. Jpn., 2, 29[21]
Nakahira, S., et al. 2014b, Astronomer's Telegram, 6012
Nakahira, S., et al. 2014c, Astronomer's Telegram, 6250
Nakahira, S., Negoro., H., Shidatsu, M., Ueda, Y., Mihara, T., Sugizaki, M., Matsuoka, M., & Onodera, T. 2014a, PASJ, 66, 84
Nakajima, M., et al. 2010, Astronomer's Telegram, 3021
Nakajima, M., et al. 2013, Astronomer's Telegram, 5205
Nakajima, M., et al. 2014a, Astronomer's Telegram, 6465
Nakajima, M., et al. 2014b, Astronomer's Telegram, 6569
Nakajima, M., et al. 2014c, Astronomer's Telegram, 6630
Negoro, H., et al. 2004, in ASP Conf. Ser., 314, Astronomical Data Analysis Software and Systems (ADASS) XIII, ed. F. Ochsenbein, M. G. Allen & D. Egret (San Francisco: ASP), 452 (N04)
Negoro, H., et al. 2008, in ASP Conf. Ser., 394, Astronomical Data Analysis Software and Systems XVII, ed. R. W. Argyle, P. S. Bunclark & J. R. Lewis (San Francisco: ASP), 597
Negoro, H., et al. 2009, Astronomer's Telegram, 2341
Negoro, H., et al. 2010a, in ASP Conf. Ser., 434, Astronomical Data Analysis Software and Systems XIX, ed. Y. Mizumoto, K.-I. Morita & M. Ohishi (San Francisco: ASP), 127
Negoro, H., et al. 2010b, Astronomer's Telegram, 2711
Negoro, H., et al. 2010c, Astronomer's Telegram, 2873
Negoro, H., et al. 2011a, Astronomer's Telegram, 3330
Negoro, H., et al. 2011b, Astronomer's Telegram, 3611
Negoro, H., et al. 2011c, Astronomer's Telegram, 3737
Negoro, H., et al. 2012a, Astronomer's Telegram, 4175
Negoro, H., et al. 2012b, Astronomer's Telegram, 4622
Negoro, H., et al. 2013a, Astronomer's Telegram, 4911
Negoro, H., et al. 2013b, Astronomer's Telegram, 4978
Negoro, H., et al. 2013c, Astronomer's Telegram, 5096
Negoro, H., et al. 2014a, Astronomer's Telegram, 5943
Negoro, H., et al. 2014b, Astronomer's Telegram, 6289
Negoro, H., & MAXI team. 2014, Suzaku-MAXI 2014: Expanding the Frontiers of the X-ray Universe, ed. M. Ishida et al. (Ehime: Ehime University), 128
Ogawa, Y., et al. 2012, GCN Circ., 14100
Ohtani, Y., Morii, M., & Shigeyama, T. 2014, ApJ, 787, 165
Onodera, T., Negoro, H., Suzuki, K., Fukushima, K., & Kennea, J. 2014, in Proc. Suzaku-MAXI 2014: Expanding the Frontiers of the X -ray Universe, ed. M. Ishida et al. (Ehime: Ehime University), 206
Ozawa, H. 2011, Master's thesis, Nihon University
Ozawa, H., Negoro, H., & Suwa, F. 2010, in Proc. 4th International MAXI Workshop, The First Year of MAXI: Monitoring Variable X-ray Sources, ed. T. Mihara & M. Serino (Sagamihara: Aoyama Gakuin University), 45
Saito, H. 2008, Master's thesis, Nihon University
Sakamoto, T., Serino, M., Kawai, N., & Yoshida, A. 2014, Suzaku-MAXI 2014: Expanding the Frontiers of the X-ray Universe, ed. M. Ishida et al. (Ehime: Ehime University), 267
Sato, R., et al. 2012, Astronomer's Telegram, 4024
Serino, M., et al. 2014a, PASJ, 66, 87
Serino, M., et al. 2014b, GCN Circ., 15882
Serino, M., et al. 2014c, Astronomer's Telegram, 6708
Serino, M., et al. 2015, PASJ, 67, 30
Serino, M., Mihara, T., Matsuoka, M., Nakahira, S., Sugizaki, M., Ueda, Yo., Kawai, N., & Ueno, S. 2012, PASJ, 64, 91
Shidatsu, M., et al. 2013, ApJ, 779, 26

[21] ⟨https://repository.exst.jaxa.jp/dspace/handle/a-is/16827⟩.

Singh, K. P., et al. 2014, Proc of SPIE, 9144, 1S
Sivakoff, G. R., Heinke, C. O., Miller-Jones, J. C. A., Altamirano, D., Kuulkers, E., & Morii, M. 2011, Astronomer's Telegram, 3393
Sootome, T., et al. 2011, Astronomer's Telegram, 3752
Strohmayer, T., & Bildsten, L. 2006, in Compact Stellar X-Ray Sources, ed. W. H. G. Lewin & M. van der Klis (Cambridge: Cambridge University Press), 113
Sugizaki, M., et al. 2011, PASJ, 63, S635
Sugizaki, M., et al. 2012, Astronomer's Telegram, 4524
Sugizaki, M., et al. 2013, PASJ, 65, 58
Sugizaki, M., Mihara, T., Kawai, N., Nakajima, M., & Matsuoka, M. 2009, Astronomer's Telegram, 2277
Suwa, F. 2012, Master's thesis, Nihon University
Suwa, F., Negoro, H., Ozawa, H., & Serino, M. 2010, in Proc.4th International MAXI Workshop The First Year of MAXI: Monitoring Variable X-ray Sources, ed. T. Mihara & M. Serino (Sagamihara: Aoyama Gakuin University), 41
Suzuki, M., et al. 2006, Nuovo Cimento B, 121, 1593
Suzuki, M., & MAXI team 2009, in Proc. 3rd International MAXI Workshop, Astrophysics with All-Sky X-Ray Observations, ed. N. Kawai et al. (Wako: Riken), 224
Tomida, H., et al. 2011, PASJ, 63, 397
Tomida, H., et al. 2013, Astronomer's Telegram, 5327
Tsuboi, Y., Higa, M., & Yamazaki, K. 2014, Suzaku-MAXI 2014: Expanding the Frontiers of the X-ray Universe, ed. M. Ishida et al. (Ehime: Ehime University), 138
Tsunemi, H., Kitamoto, S., Manabe, M., Miyamoto, S., Yamashita, K., & Nakagawa, M. 1989, PASJ, 41, 391
Tsunemi, H., Tomida, H., Katayama, H., Kimura, M., Daikyuji, A., Miyaguchi, K., & Maeda, K.2010, PASJ, 62, 1371
Tueller, J., et al. 2010, ApJS, 186, 378
Ueno, S., et al. 2009, in Proc. 3rd international MAXI Workshop, Astrophysics with All-Sky X-ray Observations, ed. N. Kawai et al., JAXA-SP-08-014E (Chofu, Tokyo: JAXA), 8
Ueno, S., et al. 2013, Astronomer's Telegram, 5320
Usui, R., et al. 2012, Astronomer's Telegram, 4140
Uzawa, A., et al. 2011, PASJ, 63, S713
Voges, W., et al. 1996, IAUC, 6420
Westergaard, N. J., et al. 2003, A&A, 411, L257
Winkler, C., et al. 2003, A&A, 411, L349
Yamamoto, T., Mihara, T., Sugizaki, M., Nakajima, M., Makishima, K., & Sasano, M. 2014, PASJ, 66, 59
Yamamoto, T., Sugizaki, M., Mihara, T., Nakajima, M., Yamaoka, K., Matsuoka, M., Morii, M., & Makishima, K. 2011, PASJ, 63, 751
Yamaoka, K., et al. 2010, Astronomer's Telegram, 2959
Yamaoka, K., et al. 2012, PASJ, 64, 32
Yamaoka, K., et al. 2014, Astronomer's Telegram, 6174
Yoshikawa, A., Yamada, S., Nakahira, S., Matsuoka, M., Negoro, H., Mihara, T., & Tamagawa, T. 2015, PASJ, 67, 11
Zauderer, B.A., et al. 2011, Nature, 476, 425